Electronic Supplementary Material (ESI) for Physical Chemistry Chemical Physics.
This journal is © the Owner Societies 2022

Electronic Supplementary Information for "π-Topology and Ultrafast Excited-State Dynamics of Remarkably Photochemically Stabilized Pentacene Derivatives with Radical Substituents"

Nishiki Minami,[a] Kohei Yoshida,[a] Keijiro Maeguchi,[a] Ken Kato,[a]
Akihiro Shimizu,[a] Genta Kashima,[a] Masazumi Fujiwara,[a]
Chiasa Uragami,[b] Hideki Hashimoto,[b] and Yoshio Teki*[a]

[a] *Division of Molecular Materials Science/Department of Chemistry,*
Graduate School of Science
Osaka City University
3-3-138 Sugimoto, Sumiyoshi-ku, Osaka 558-8585, Japan

[b] *Department of Applied Chemistry for Environment,*
Graduate School of Science and Technology
Kwansei Gakuin University
Sanda, Hyogo 669-1337, Japan

*To whom Correspondence should be addressed.

Fax: (+)81-6-6605-2559

E-mail: teki@osaka-cu.ac.jp

Contents

Detailed Synthetic Procedures

General experimental details. 1*m* and **1*p*** were synthesized from 6,13-pentacenedione as the starting material according to the procedures shown in Schemes S1 (Scheme 1) and S2, respectively. The syntheses of compounds **2**, **3** and **4** were accomplished following reported literature protocols [S1, S2] with some modifications. 6,13-pentacenedione, other reagents and solvents were purchased from either Sigma-Aldrich Co., Inc., Kanto Chemical Co., Inc., Tokyo Kasei Kogyo Co., Ltd., Merck & Co., Inc., Wako Pure Chemical Ind., Ltd. and Nacalai Tesque Co., Ltd., and used without further purification unless otherwise indicated. Melting points were determined using an AS ONE ATM-1 melting point apparatus and were uncorrected. ^{1}H NMR and ^{13}C NMR spectra were recorded on a Bruker AVANCE300N (300 MHz, 75 MHz), AVANCE400 (400 MHz, 100 MHz), or AVANCE600 (600 MHz, 150 MHz) spectrometer. Chemical shifts of ^{1}H NMR and ^{13}C NMR were reported in parts per million (ppm, δ) relative to those of tetramethylsilane (δ = 0 ppm) or solvent residual signals (δ = 7.26 (^{1}H) and 77.1 ppm (^{13}C) in $CDCl_3$, δ = 5.32 (^{1}H) and 53.84 ppm (^{13}C) in CD_2Cl_2, and δ = 2.49 (^{1}H) and 39.5 ppm (^{13}C) in $(CD_3)_2SO$). High-resolution mass spectra (HRMS) were obtained on a JEOL JMS-700(S) using fast atom bombardment (FAB) method and on a JEOL AccuTOF LC-plus JMS-T100LP for direct analysis in real time (DART). All reactions were monitored by thin-layer chromatography (TLC), which was performed on silica gel-precoated plates (Merck silica gel 60 F_{254}) and visualized by using a UV lamp. Daiso IR-60 1002W (40/63 mm) was used for the flash column chromatography. Because the pentacene framework is known to be unstable under ambient light, the syntheses of the compounds with the pentacene framework were carried out in the dark, and the experimental apparatus was covered with the aluminum foil.

(i) Synthesis of 1*m*

Synthesis of **1*m*** involved multiple steps as shown in Scheme S1 (Scheme 1).

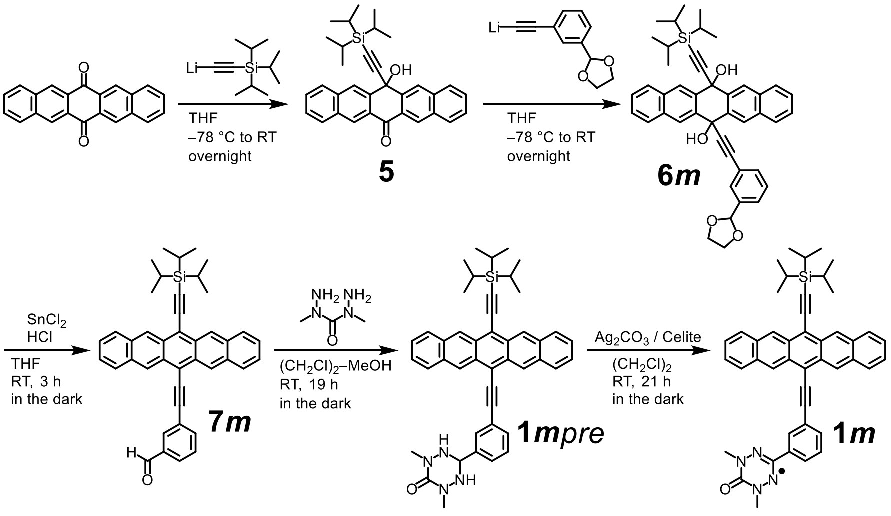

Scheme S1. Synthetic route of **1*m***

13-hydroxy-13-((triisopropylsilyl)ethynyl)pentacene-6(13H)-one (5)

5 was synthesized according to the procedures described in the literature[S3] with some modifications. To triisopropylsilylacetylene (5.73 g, 31.4 mmol) in dry THF (100 mL) was added dropwise *n*-BuLi (20 mL, 25 mmol, 1.6 mol L^{-1} in hexane) at –78 °C under argon. After stirring at –78 °C for 30 min, 6,13-pentacenedione (9.68 g, 31.4 mmol) was added to the solution. The mixture was warmed to room temperature and stirred for 19 h. The solution was washed with satd. NH_4Cl aq. (50 mL × 3) and satd. NaCl aq. (40 mL × 2). The organic layer was dried over anhydrous $MgSO_4$ and concentrated under reduced pressure. The residual THF was removed by $(CH_2Cl)_2$ under reduced pressure at 3 times. Finally, the residue was purified by silica-gel column chromatography (eluent: CH_2Cl_2) to afford **5** as a yellow powder (6.51 g, 53% yield). mp: 212°C;^{1}H NMR (300 MHz, $CDCl_3$): δ/ppm 8.86 (s, 2H), 8.74 (s, 2H), 8.07 (d, J = 8.0 Hz, 2H), 7.95 (d, J = 8.0 Hz, 2H), 7.68-7.58 (m, 4H), 2.93 (s, 1H), 1.23-1.17 (m, 21H); ^{13}C NMR (100 MHz, $CDCl_3$): δ/ppm 184.4 (CO), 138.8, 135.7, 132.8, 129.8, 129.7, 128.9, 128.4, 128.2, 127.4, 127.3, 108.3, 90.0, 68.6, 18.7, 11.3 ; HRMS (*m*/*z*): $[M+Na]^+$ calcd for 513.22258; found 513.22391.

6-((3-(1,3-dioxolan-2-yl)phenyl)ethynyl)-13-((triisopropylsilyl)ethynyl)-6,13-dihydropentacene-6,13-diol) (6*m*)

To 2-(3-ethynylphenyl)-1,3-dioxolane (4.21 g, 24.2 mmol) in dry THF (60 mL) was added dropwise *n*-BuLi (20 mL, 25 mmol, 1.6 mol L^{-1} in hexane) at –78 °C under argon. After stirring at –78 °C for 30 min, **5** (2.93 g, 5.96 mmol) was added to the solution. The mixture was warmed to room temperature and stirred for 17 h. The solution was washed with satd. NH_4Cl aq. (50 mL × 3) and satd. NaCl aq. (40 mL × 2). The organic layer was dried over anhydrous $MgSO_4$ and concentrated under reduced pressure. The residue was purified using silica-gel column chromatography (eluents: CH_2Cl_2/ethyl acetate = 25/1). The fraction was concentrated under reduced pressure and was purified using silica-gel column chromatography (eluent: $(CH_2Cl)_2$) to afford **6*m*** as a colorless powder (1.57 g, 40% yield). mp: 107°C; ^{1}H NMR (300 MHz, $CDCl_3$): δ/ppm 8.78 (s, 2H), 8.62 (s, 2H), 7.99-7.90 (m, 4H), 7.57-7.51 (m, 6H), 7.39-7.36 (m, 2H), 5.72 (s, 1H), 4.08-3.95 (m, 4H), 3.45 (s, 1H), 3.39 (s, 1H), 1.20-1.18 (m, 21H) ; ^{13}C NMR (150 MHz, $CDCl_3$): δ/ppm 138.3, 137.1, 135.3, 133.3, 133.1, 132.4, 129.7, 128.3, 128.2, 128.2, 127.0, 126.9, 126.8, 126.8, 125.2, 122.0, 108.3, 103.0, 92.1, 90.5, 86.8, 70.7, 68.8, 65.2, 18.8, 11.3; HRMS (*m*/*z*): $[M+Na]^+$ calcd for $C_{44}H_{44}O_4SiNa$, 687.29065; found 687.29078.

3-((13-((triisopropylsilyl)ethynyl)pentacen-6-yl)ethynyl)benzaldehyde (7*m*)

$SnCl_2$ in conc. HCl (7.4 mol L^{-1}, 5 mL) was added to **6*m*** (711 mg, 1.07 mmol) in THF (20 mL) at 0 °C. The mixture was stirred for 3 h. Satd. $NaHCO_3$ aq. was added to the solution to achieve a pH of 7.5. The solution was washed with satd. NaCl aq. (40 mL × 2). The reaction suspension was filtrated, and the residue was washed with ethanol (1 mL × 3) and hexane (1 mL × 3). The residue was purified using silica-gel column chromatography (eluent: CH_2Cl_2/hexane = 2/1) to afford ***7m*** as a greenish blue powder (464 mg, 74% yield). mp: 219 °C; ^{1}H NMR (300 MHz, $CDCl_3$): δ/ppm 10.2 (s, 1H), 9.34 (s, 2H), 9.26 (s, 2H), 8.39 (s, 1H), 8.15 (d, J = 8.0 Hz, 1H), 8.09-8.06 (m, 2H), 8.00-7.97 (m, 3H), 7.72 (t, J = 8.0 Hz, 1H), 7.47-7.42 (m, 4H), 1.42-1.38 (m, 21H); ^{13}C NMR (150 MHz, $CDCl_3$): δ/ppm 191.6 (CHO), 137.2, 136.7, 132.8, 132.3, 132.3, 130.5, 130.2, 129.4, 129.4, 128.7, 128.6, 126.5, 126.2, 126.1, 125.7, 124.8, 119.1, 117.0, 107.6, 104.6, 102.6, 89.4, 19.0, 11.7; HRMS (m/z): $[M]^+$ calcd for $C_{42}H_{38}OSi$, 586.26919; found 586.27049.

2,4-dimethyl-6-(3-((13-((triisopropylsilyl)ethynyl)pentacen-6-yl)ethynyl)phenyl)-1,2,4,5-tetrazinan-3-one (1*mpre*)

A mixture of ***7m*** (106 mg, 0.181 mmol) and 1,3-diamino-1,3-dimethylurea (100 mg, 0.849 mmol) in $(CH_2Cl)_2$ (3 mL) and methanol (15 mL) was stirred at room temperature for 19 h under argon in the dark. The solvents were removed under reduced pressure. To remove the unreacted 1,3-diamino-1,3-dimethylurea, the resulting solid was suspended in MeOH and filtrated to afford **1*m****pre* as a greenish blue powder (102 mg, 82% yield). mp: 211 °C; ^{1}H NMR (300 MHz, $CDCl_3$): δ/ppm 9.33 (s, 2H), 9.27 (s, 2H), 8.08-8.04 (m, 3H), 8.00-7.97 (m, 2H), 7.89 (d, J = 8.0 Hz, 1H), 7.67 (d, J = 8.0 Hz, 1H), 7.56 (t, J = 8.0 Hz, 1H), 7.46-7.40 (m, 4H), 5.20 (brd, 1H), 4.52 (brd, 2H), 3.26 (s, 6H), 1.41-1.36 (m, 21H); ^{13}C NMR (100 MHz, $CDCl_3$): δ/ppm 155.5 (CO), 135.9, 132.3, 132.3, 132.0, 130.6, 130.3, 129.8, 129.0, 128.7, 128.6, 126.9, 126.5, 126.2, 126.1, 125.9, 124.1, 118.7, 117.6, 107.5, 104.7, 103.9, 88.4, 69.1, 38.2, 19.0, 11.7; HRMS (m/z): $[M]^+$ calcd for $C_{45}H_{46}N_4OSi$, 686.34409; found 686.34459.

2,4-dimethyl-6-(3-((13-((triisopropylsilyl)ethynyl)pentacene-6-yl)ethynyl)phenyl)erdazyl-3-one (1*m*)

To **1*m****pre* (100 mg, 0.146 mmol) was added Ag_2CO_3 on celite (48 wt%, 588 mg, 1.02 mmol) in $(CH_2Cl)_2$ (20 mL) and stirred at room temperature for 21 h in the dark. The mixture was purified by column chromatography using 6wt% water-added alumina (eluent, hexane/CH_2Cl_2 = 1/1). The fractions containing **1*m*** were collected and concentrated under reduced pressure. Hexane was added to the concentrated solution. The resulting crystals were filtrated to afford **1*m*** as a greenish blue powder (19 mg, 19% yield). mp: > 300 °C; HRMS (m/z): $[M]^+$ calcd for $C_{45}H_{43}N_4OSi$, 683.32061; found 683.32048.

(ii) Syntheses of 1*p*

7*p* was synthesized following procedures similar to that reported in the literature.[S4]

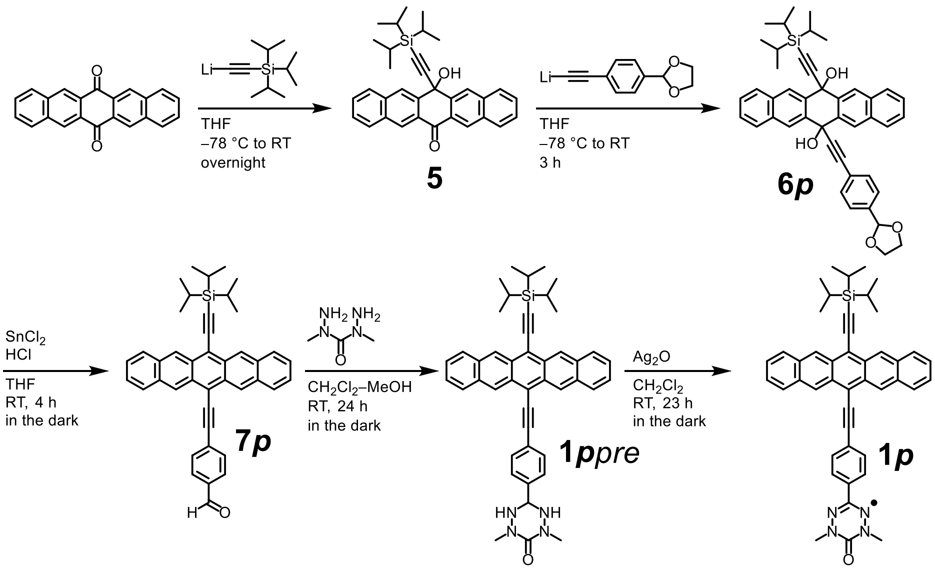

Scheme S2. Synthetic route of **1*p***

6-((4-(1,3-dioxolan-2-yl)phenyl)ethynyl)-13-((triisopropylsilyl)ethynyl)-6,13-dihydropentacene-6,13-diol (6*p*)

To 2-(4-ethynylphenyl)-1,3-dioxolane (559 mg, 3.21 mmol) in dry THF (10 mL) was added dropwise *n*-BuLi (2.25 mL, 3.51 mmol, 1.56 mol L^{-1} in hexane) at –78 °C under argon. After stirring at –78 °C for 30 min, **5** (528 mg, 1.08 mmol) was added to the solution. The mixture was warmed to room temperature and stirred for 3 h. The mixture was poured into satd. NH_4Cl aq. (60 mL) and extracted with CH_2Cl_2 (30 mL × 3). The organic layer was washed with satd. NaCl (60 mL) aq. The organic layer was dried over anhydrous Na_2SO_4, filtered, and then concentrated under a reduced pressure. The obtained residue was purified by silica-gel column chromatography (eluents: hexane/CH_2Cl_2 =2/1) to afford **6*p*** as a pale-yellow solid (666 mg, 93% yield). ^{1}H NMR (400 MHz, $CDCl_3$): δ/ppm 8.78 (s, 2H), 8.62 (s, 2H), 7.98–7.91 (m, 4H), 7.56–7.54 (m, 4H), 7.39 (d, J = 8.2 Hz, 2H), 7.34 (d, J = 8.2 Hz, 2H), 5.75 (s, 1H), 4.08–3.97 (m, 4H), 3.45 (s, 1H), 3.38 (s, 1H), 1.24–1.18 (m, 21H); HRMS (*m*/*z*): $[M+Na]^+$ calcd for $C_{44}H_{44}NaO_4Si$, 687.2907; found 687.2891.

4-((13-((triisopropylsilyl)ethynyl)pentacene-6-yl)ethynyl)benzaldehyde (7*p*)

$SnCl_2$ in conc. HCl (3.7 mol L^{-1}, 1.5 mL) was added to **6*p*** (666 mg, 1.00 mmol) in THF (25 mL) at room temperature. After stirring for 4 h, the reaction mixture was poured into satd. $NaHCO_3$ aq. (100 mL) and extracted with CH_2Cl_2 (80 mL × 4). The organic layer was washed with satd. NaCl aq. (300 mL). The organic layer was dried over anhydrous Na_2SO_4, filtered, and then concentrated under a reduced pressure. The obtained residue was purified by silica-gel column chromatography (eluent: hexane/CH_2Cl_2 =1/1) to afford ***7p*** as a greenish blue solid (501 mg, 85% yield). ^{1}H NMR (400 MHz, $CDCl_3$): δ/ppm 10.1 (s, 1H), 9.33 (s, 2H), 9.23 (s, 2H), 8.07–7.97 (m, 8H, the signals are including phenylene group (4H) and pentacene moiety (4H)), 7.46–7.43 (m, 4H), 1.41–1.37 (m, 21H); HRMS (*m*/*z*): $[M]^+$ calcd for $C_{42}H_{38}OSi$, 586.2692; found 586.2715.

2,4-dimethyl-6-(4-((13-((triisopropylsilyl)ethynyl)pentacene-6-yl)ethynyl)phenyl)-1,2,4,5-tetrazinan-3-one (1*ppre*)

A mixture of ***7p*** (501 mg, 0.85 mmol) and 1,3-diamino-1,3-dimethylurea (415 mg,3.51 mmol) in CH_2Cl_2 (20 mL) and methanol (20 mL) was stirred at room temperature for 24 h under argon in the dark. The reaction mixture was concentrated under reduced pressure. The residue was washed with cooled methanol to give **1*ppre*** as a blue solid (539 mg, 92%). mp: 191 °C (Decomp); ^{1}H NMR (400 MHz, $CDCl_3$): δ/ppm 9.34 (s, 2H), 9.28 (s, 2H), 8.08–8.05 (m, 2H), 8.00–7.98 (m, 2H), 7.93 (d, J = 8.2 Hz, 2H), 7.74 (d, J = 8.2 Hz, 2H), 7.45–7.41 (m, 4H), 5.19 (t, J = 9.1 Hz, 1H), 4.49 (d, J = 9.1 Hz, 2H), 3.23 (s, 6H), 1.43–1.36 (m, 21H); ^{13}C NMR (100 MHz, $CDCl_3$): δ/ppm 155.4, 135.6, 132.3, 132.2, 131.9, 130.6, 130.1, 128.7, 128.6, 126.8, 126.4, 126.1, 126.1, 125.9, 124.0, 118.5, 117.7, 107.4, 104.8, 103.9, 88.7, 69.1, 38.2, 19.2, 11.8; HRMS (*m/z*): $[M+Na]^+$ calcd for $C_{45}H_{46}N_4NaOSi$, 709.3339; found 709.3328.

2,4-dimethyl-6-(4-((13-((triisopropylsilyl)ethynyl)pentacene-6-yl)ethynyl)phenyl)-erdazyl-3-one (1*p*)

A mixture of **1*ppre*** (305 mg, 0.44 mmol) and Ag_2O (515 mg, 2.22 mmol) in CH_2Cl_2 (30 mL) was stirred at room temperature for 23 h in the dark. The reaction mixture was passed through a Celite pad, and the filtrate was concentrated under reduced pressure until a little amount of CH_2Cl_2 solution. The obtained crude solution was purified by column chromatography on a 6wt% water-impregnated silica-gel (eluent: hexane/CH_2Cl_2 =1/1). Fractions containing ***1p*** were collected and concentrated (~1/5 volume) under reduced pressure. The generated precipitate was filtrated to give ***1p*** as a blue solid (120 mg, 40% yield). mp: > 300 °C; HRMS (*m*/*z*): $[M]^+$ calcd for $C_{45}H_{43}N_4OSi$, 683.3206; found 683.3195.

NMR data of the compounds

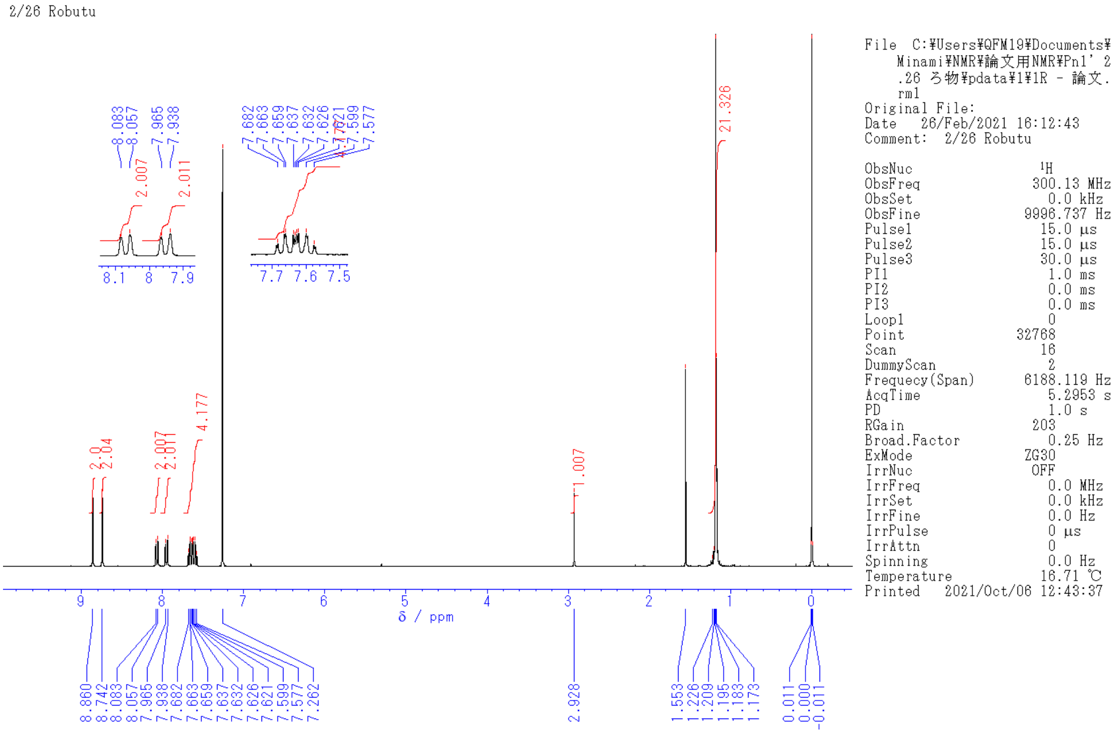

```
File  C:¥Users¥QFM19¥Documents¥
    Minami¥NMR¥論文用NMR¥Pn1' 2
    .26 ろ物¥pdata¥1¥1R - 論文.
    rml
Original File:
Date   26/Feb/2021 16:12:43
Comment:  2/26 Robutu

ObsNuc                  1H
ObsFreq               300.13 MHz
ObsSet                  0.0 kHz
ObsFine              9996.737 Hz
Pulse1                 15.0 µs
Pulse2                 15.0 µs
Pulse3                 30.0 µs
PI1                     1.0 ms
PI2                     0.0 ms
PI3                     0.0 ms
Loop1                   0
Point               32768
Scan                   16
DummyScan               2
Frequecy(Span)       6188.119 Hz
AcqTime                 5.2953 s
PD                      1.0 s
RGain                 203
Broad.Factor            0.25 Hz
ExMode                ZG30
IrrNuc                 OFF
IrrFreq                 0.0 MHz
IrrSet                  0.0 kHz
IrrFine                 0.0 Hz
IrrPulse                0 µs
IrrAttn                 0
Spinning                0.0 Hz
Temperature            16.71 ℃
Printed    2021/Oct/06 12:43:37
```

Figure S1. ^{1}H NMR spectra of **5**.

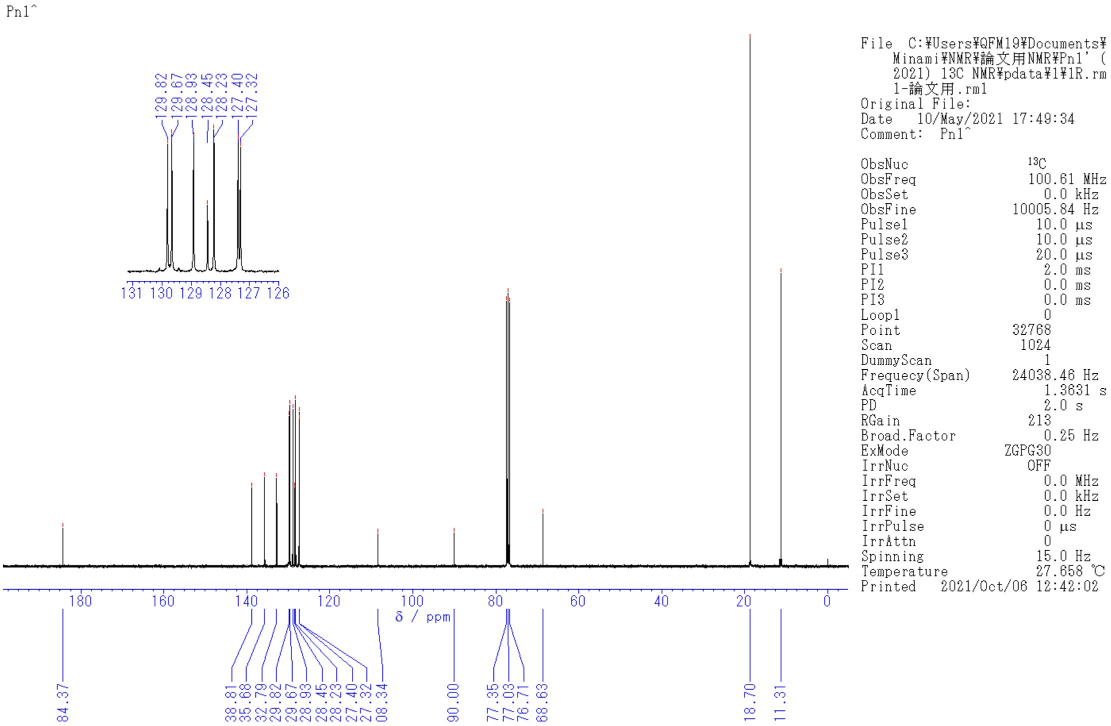

```
File  C:¥Users¥QFM19¥Documents¥
    Minami¥NMR¥論文用NMR¥Pn1' (
    2021) 13C NMR¥pdata¥1¥1R.rm
    1-論文用.rml
Original File:
Date   10/May/2021 17:49:34
Comment:  Pn1^

ObsNuc                  13C
ObsFreq               100.61 MHz
ObsSet                  0.0 kHz
ObsFine             10005.84 Hz
Pulse1                 10.0 µs
Pulse2                 10.0 µs
Pulse3                 20.0 µs
PI1                     2.0 ms
PI2                     0.0 ms
PI3                     0.0 ms
Loop1                   0
Point               32768
Scan                 1024
DummyScan               1
Frequecy(Span)      24038.46 Hz
AcqTime                 1.3631 s
PD                      2.0 s
RGain                 213
Broad.Factor            0.25 Hz
ExMode               ZGPG30
IrrNuc                 OFF
IrrFreq                 0.0 MHz
IrrSet                  0.0 kHz
IrrFine                 0.0 Hz
IrrPulse                0 µs
IrrAttn                 0
Spinning               15.0 Hz
Temperature            27.658 ℃
Printed    2021/Oct/06 12:42:02
```

Figure S2. ^{13}C NMR spectra of **5**.

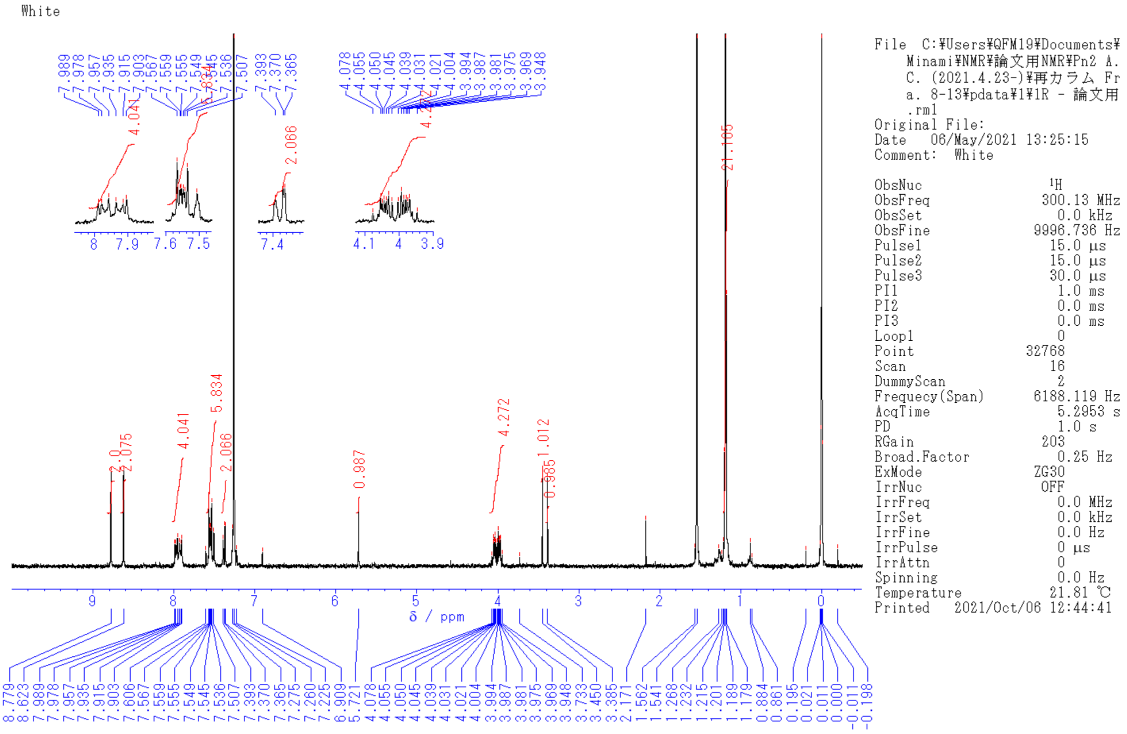

Figure S3. ^{1}H NMR spectra of **6*m***.

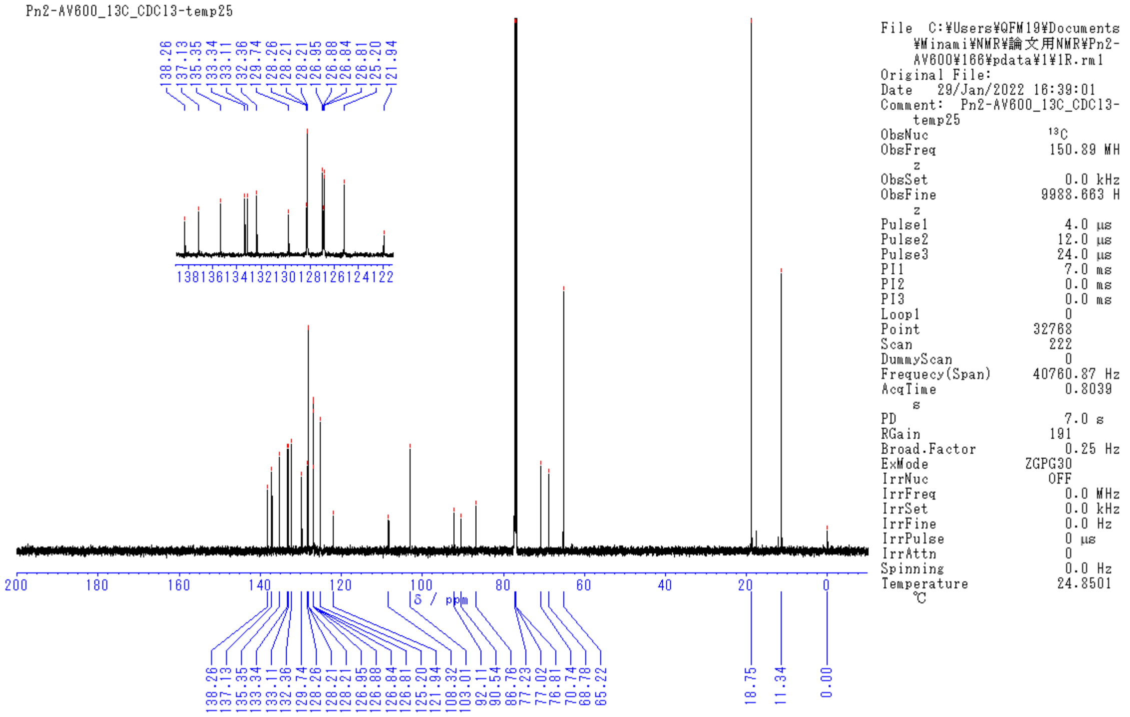

Figure S4. ^{13}C NMR spectra of **6*m***.

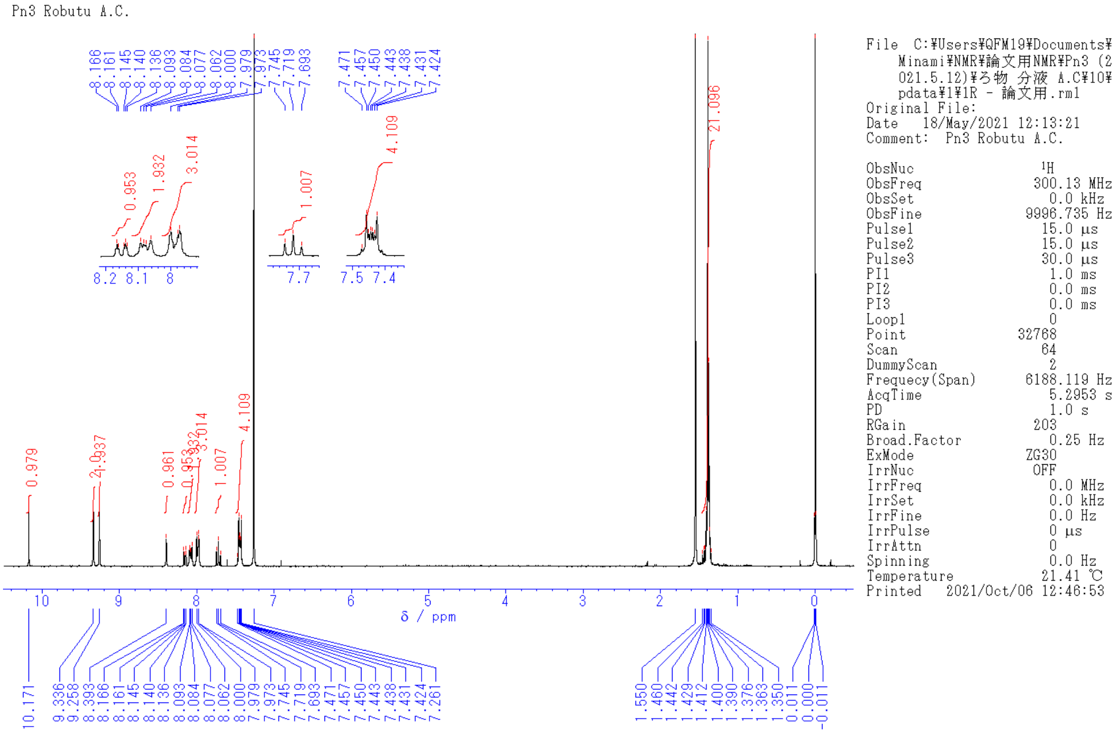

```
File  C:¥Users¥QFM19¥Documents¥
    Minami¥NMR¥論文用NMR¥Pn3 (2
    021.5.12)¥ろ物 分液 A.C¥10¥
    pdata¥1¥1R - 論文用.rml
Original File:
Date     18/May/2021 12:13:21
Comment:  Pn3 Robutu A.C.

ObsNuc                  ¹H
ObsFreq              300.13 MHz
ObsSet                  0.0 kHz
ObsFine            9996.735 Hz
Pulse1                 15.0 μs
Pulse2                 15.0 μs
Pulse3                 30.0 μs
PI1                     1.0 ms
PI2                     0.0 ms
PI3                     0.0 ms
Loop1                   0
Point               32768
Scan                   64
DummyScan               2
Frequecy(Span)     6188.119 Hz
AcqTime              5.2953 s
PD                      1.0 s
RGain                 203
Broad.Factor           0.25 Hz
ExMode               ZG30
IrrNuc                OFF
IrrFreq                 0.0 MHz
IrrSet                  0.0 kHz
IrrFine                 0.0 Hz
IrrPulse                0 μs
IrrAttn                 0
Spinning                0.0 Hz
Temperature           21.41 ℃
Printed    2021/Oct/06 12:46:53
```

Figure S5. ^{1}H NMR spectra of **7*m***.

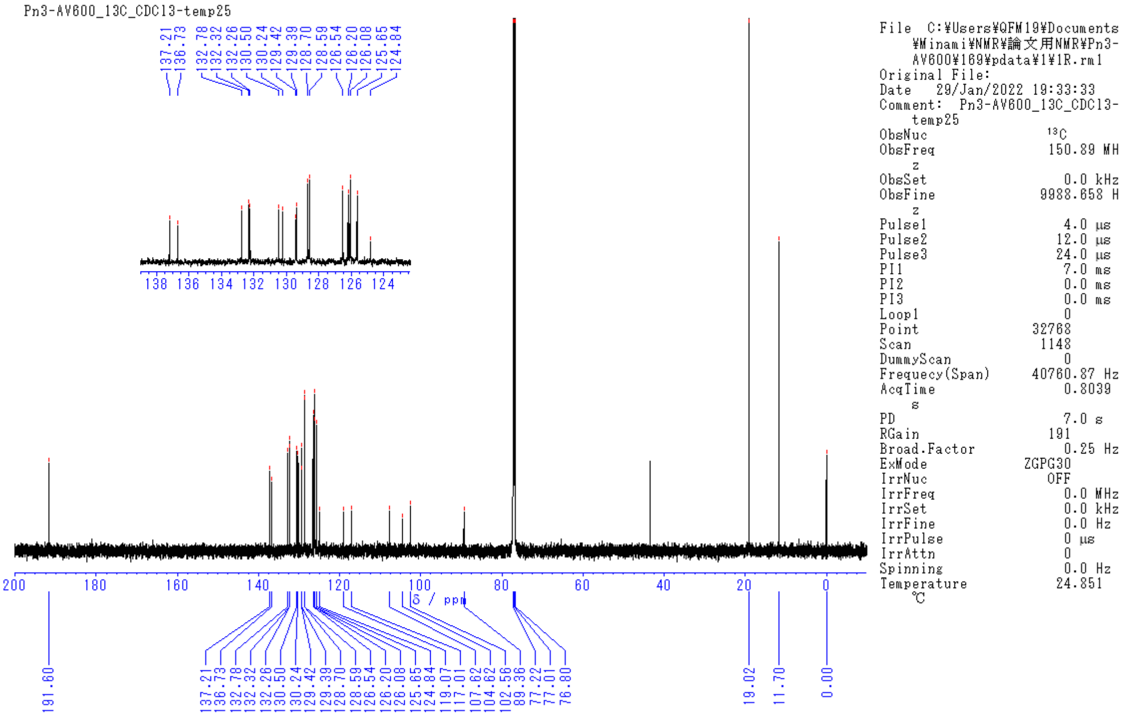

```
File  C:¥Users¥QFM19¥Documents
    ¥Minami¥NMR¥論文用NMR¥Pn3-
    AV600¥169¥pdata¥1¥1R.rml
Original File:
Date    29/Jan/2022 19:33:33
Comment:  Pn3-AV600_13C_CDCl3-
    temp25
ObsNuc                 ¹³C
ObsFreq              150.89 MH
    z
ObsSet                  0.0 kHz
ObsFine            9988.658 H
    z
Pulse1                  4.0 μs
Pulse2                 12.0 μs
Pulse3                 24.0 μs
PI1                     7.0 ms
PI2                     0.0 ms
PI3                     0.0 ms
Loop1                   0
Point               32768
Scan                 1148
DummyScan               0
Frequecy(Span)     40760.87 Hz
AcqTime              0.3039
    s
PD                      7.0 s
RGain                 191
Broad.Factor           0.25 Hz
ExMode              ZGPG30
IrrNuc                OFF
IrrFreq                 0.0 MHz
IrrSet                  0.0 kHz
IrrFine                 0.0 Hz
IrrPulse                0 μs
IrrAttn                 0
Spinning                0.0 Hz
Temperature          24.851
    ℃
```

Figure S6. ^{13}C NMR spectra of **7*m***.

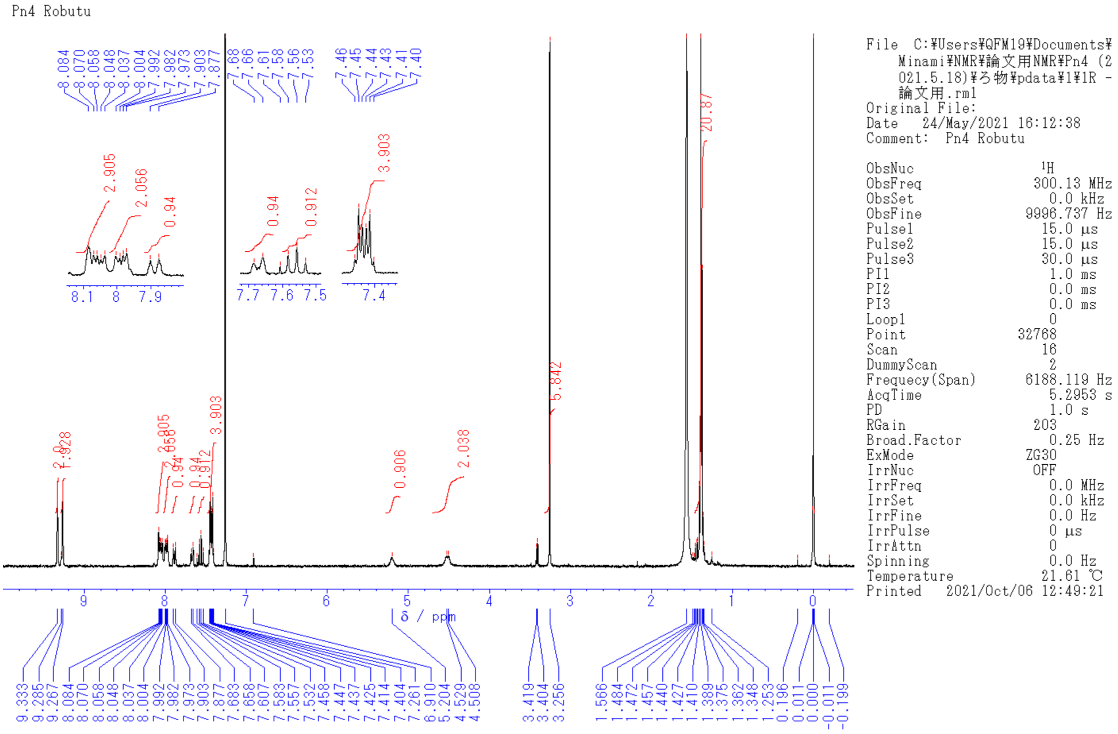

```
File  C:¥Users¥QFM19¥Documents¥
    Minami¥NMR¥論文用NMR¥Pn4 (2
    021.5.18)¥ろ物¥pdata¥1¥1R -
    論文用.rml
Original File:
Date   24/May/2021 16:12:38
Comment:  Pn4 Robutu

ObsNuc                 1H
ObsFreq               300.13 MHz
ObsSet                  0.0 kHz
ObsFine              9996.737 Hz
Pulse1                 15.0 µs
Pulse2                 15.0 µs
Pulse3                 30.0 µs
PI1                     1.0 ms
PI2                     0.0 ms
PI3                     0.0 ms
Loop1                   0
Point               32768
Scan                   16
DummyScan               2
Frequecy(Span)       6188.119 Hz
AcqTime                 5.2953 s
PD                      1.0 s
RGain                 203
Broad.Factor            0.25 Hz
ExMode               ZG30
IrrNuc                OFF
IrrFreq                 0.0 MHz
IrrSet                  0.0 kHz
IrrFine                 0.0 Hz
IrrPulse                0 µs
IrrAttn                 0
Spinning                0.0 Hz
Temperature            21.61 ℃
Printed   2021/Oct/06 12:49:21
```

Figure S7. ^{1}H NMR spectra of **1*mpre***.

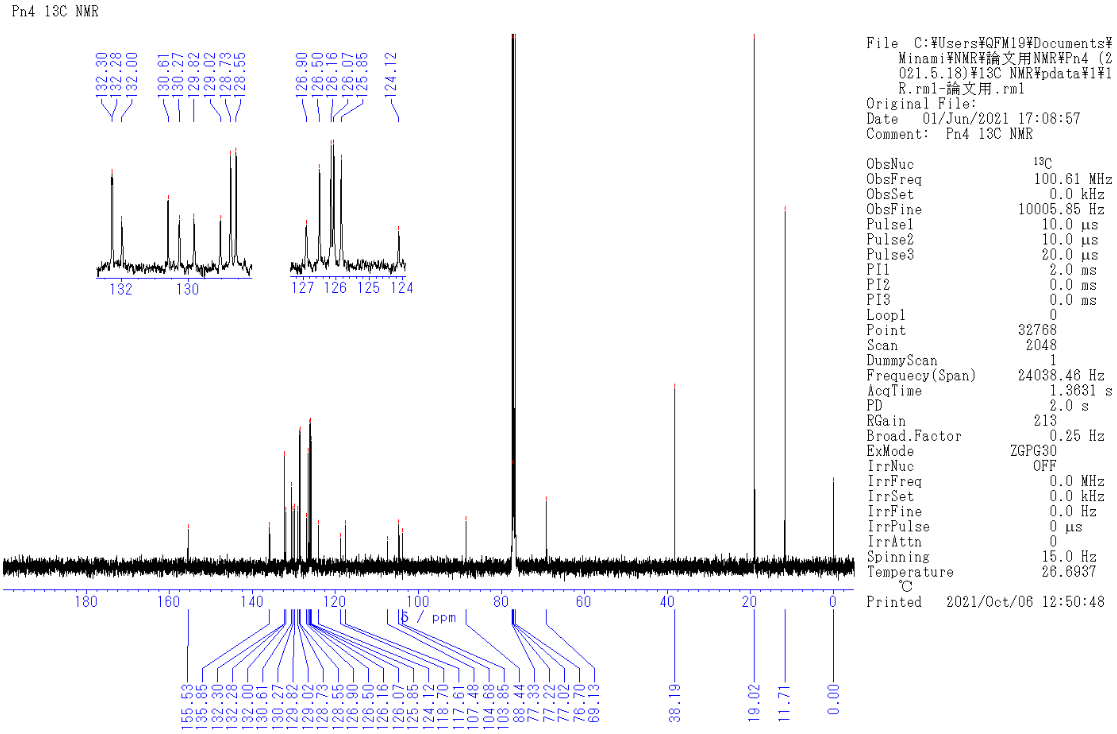

```
File  C:¥Users¥QFM19¥Documents¥
    Minami¥NMR¥論文用NMR¥Pn4 (2
    021.5.18)¥13C NMR¥pdata¥1¥1
    R.rml-論文用.rml
Original File:
Date   01/Jun/2021 17:08:57
Comment:  Pn4 13C NMR

ObsNuc                 13C
ObsFreq               100.61 MHz
ObsSet                  0.0 kHz
ObsFine             10005.85 Hz
Pulse1                 10.0 µs
Pulse2                 10.0 µs
Pulse3                 20.0 µs
PI1                     2.0 ms
PI2                     0.0 ms
PI3                     0.0 ms
Loop1                   0
Point               32768
Scan                 2048
DummyScan               1
Frequecy(Span)      24038.46 Hz
AcqTime                 1.3631 s
PD                      2.0 s
RGain                 213
Broad.Factor            0.25 Hz
ExMode             ZGPG30
IrrNuc                OFF
IrrFreq                 0.0 MHz
IrrSet                  0.0 kHz
IrrFine                 0.0 Hz
IrrPulse                0 µs
IrrAttn                 0
Spinning               15.0 Hz
Temperature            26.6937
    ℃
Printed   2021/Oct/06 12:50:48
```

Figure S8. ^{13}C NMR spectra of **1*mpre***.

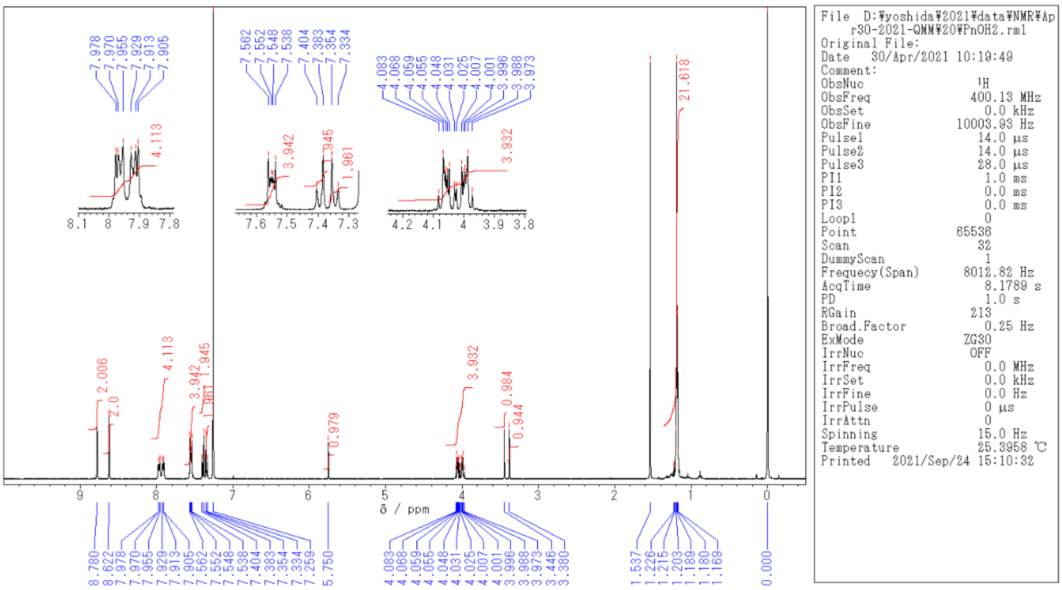

Figure S9. ^{1}H NMR spectrum of **6*p***.

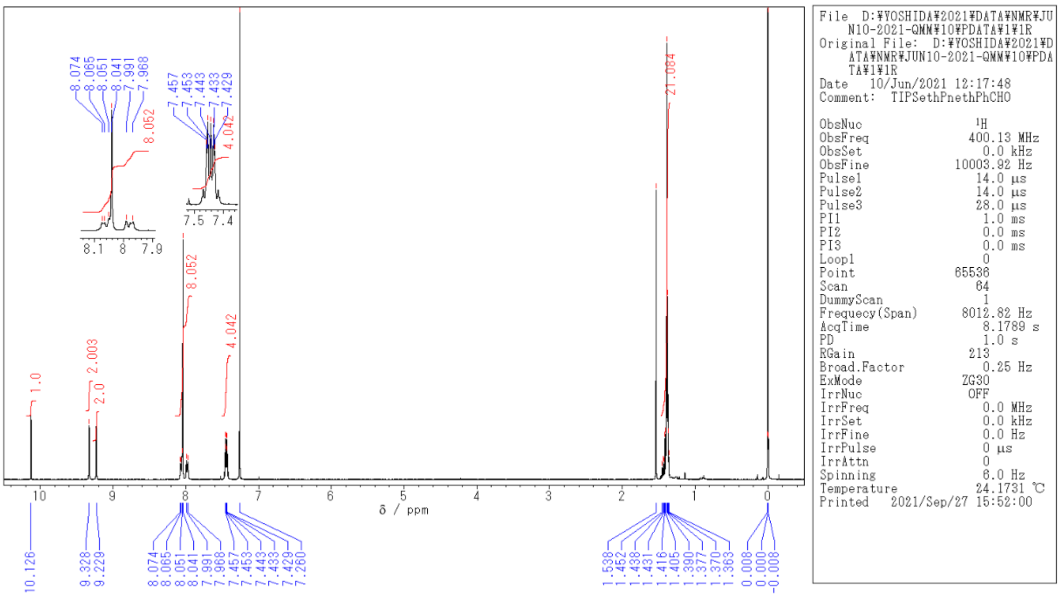

Figure S10. ^{1}H NMR spectrum of **7*p***.

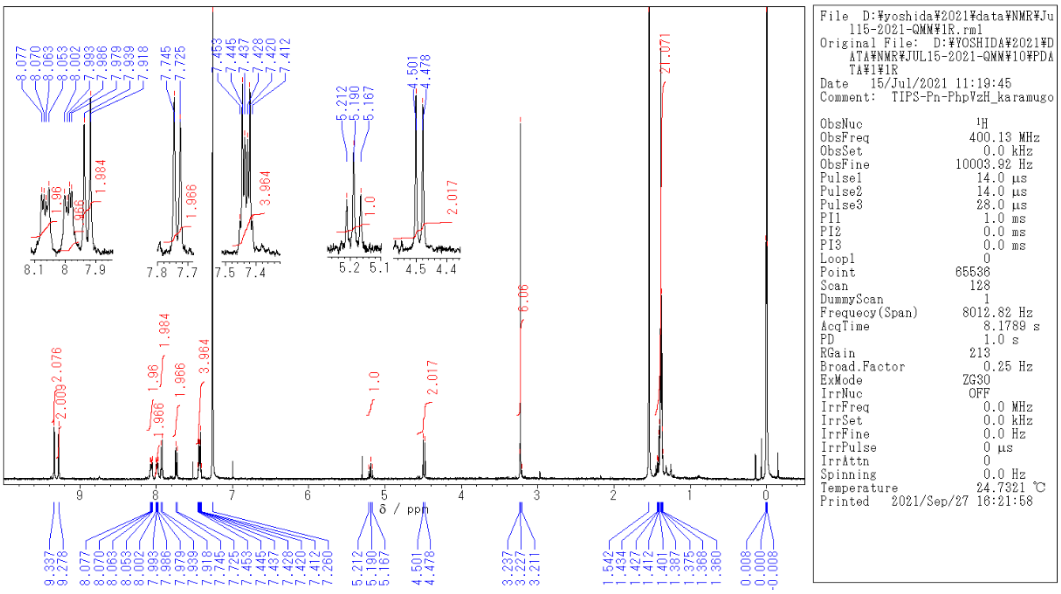

```
File  D:¥yoshida¥2021¥data¥NMR¥Ju
    l15-2021-QMM¥1R.rml
Original File:  D:¥YOSHIDA¥2021¥D
    ATA¥NMR¥JUL15-2021-QMM¥10¥PDA
    TA¥1¥1R
Date   15/Jul/2021 11:19:45
Comment:  TIPS-Pn-PhpVzH_karamugo

ObsNuc                  ¹H
ObsFreq                400.13 MHz
ObsSet                   0.0 kHz
ObsFine              10003.92 Hz
Pulse1                  14.0 µs
Pulse2                  14.0 µs
Pulse3                  28.0 µs
PI1                      1.0 ms
PI2                      0.0 ms
PI3                      0.0 ms
Loop1                    0
Point                65536
Scan                   128
DummyScan                1
Frequecy(Span)        8012.82 Hz
AcqTime                  8.1789 s
PD                       1.0 s
RGain                  213
Broad.Factor             0.25 Hz
ExMode                ZG30
IrrNuc                 OFF
IrrFreq                  0.0 MHz
IrrSet                   0.0 kHz
IrrFine                  0.0 Hz
IrrPulse                 0 µs
IrrAttn                  0
Spinning                 0.0 Hz
Temperature             24.7321 ℃
Printed   2021/Sep/27 16:21:58
```

Figure S11. ^{1}H NMR spectrum of **1*ppre***.

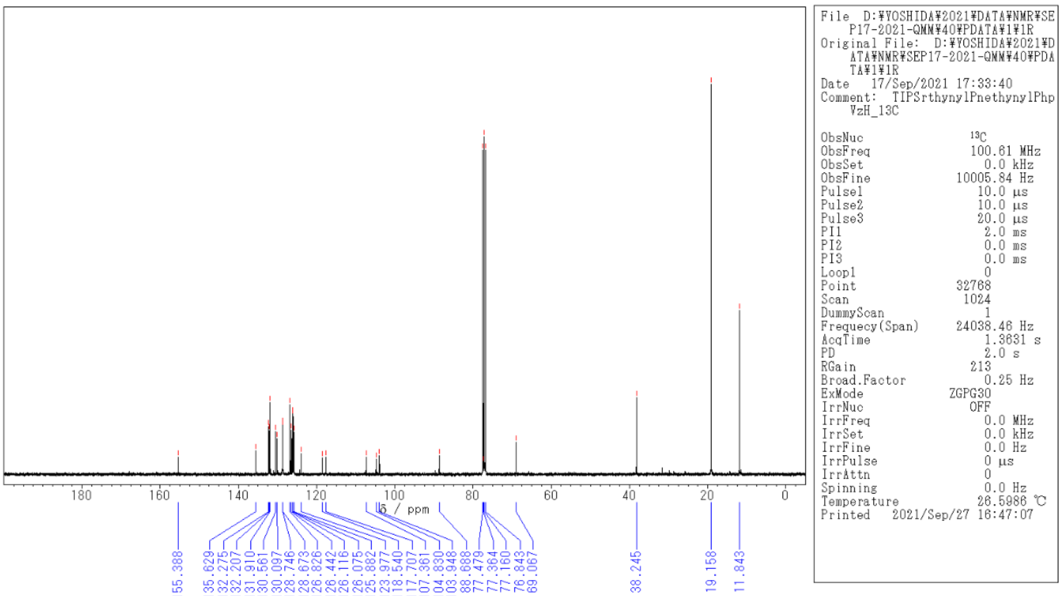

```
File  D:¥YOSHIDA¥2021¥DATA¥NMR¥SE
    P17-2021-QMM¥40¥PDATA¥1¥1R
Original File:  D:¥YOSHIDA¥2021¥D
    ATA¥NMR¥SEP17-2021-QMM¥40¥PDA
    TA¥1¥1R
Date   17/Sep/2021 17:33:40
Comment:  TIPSrthynylPnethynylPhp
    VzH_13C

ObsNuc                  ¹³C
ObsFreq                100.61 MHz
ObsSet                   0.0 kHz
ObsFine              10005.84 Hz
Pulse1                  10.0 µs
Pulse2                  10.0 µs
Pulse3                  20.0 µs
PI1                      2.0 ms
PI2                      0.0 ms
PI3                      0.0 ms
Loop1                    0
Point                32768
Scan                  1024
DummyScan                1
Frequecy(Span)       24038.46 Hz
AcqTime                  1.3631 s
PD                       2.0 s
RGain                  213
Broad.Factor             0.25 Hz
ExMode              ZGPG30
IrrNuc                 OFF
IrrFreq                  0.0 MHz
IrrSet                   0.0 kHz
IrrFine                  0.0 Hz
IrrPulse                 0 µs
IrrAttn                  0
Spinning                 0.0 Hz
Temperature             26.5986 ℃
Printed   2021/Sep/27 16:47:07
```

Figure S12. ^{13}C NMR spectrum of **1*ppre***.

Electron Spin Resonance (ESR) Measurements

ESR spectra of **1*m*** and **1*p*** were measured in degassed toluene (degassing was done by Ar bubbling for a few min) at room temperature using a JEOL JES-TE300 ESR spectrometer. Typical experimental parameters are as follows; 100 kHz magnetic field modulation, 0.01 mT modulation width, and 0.3 sec time constant. The microwave frequency and power were 9.44244 and 9.44537 GHz for **1*m*** and **1*p***, respectively, and the power was 1.00 mW for both.

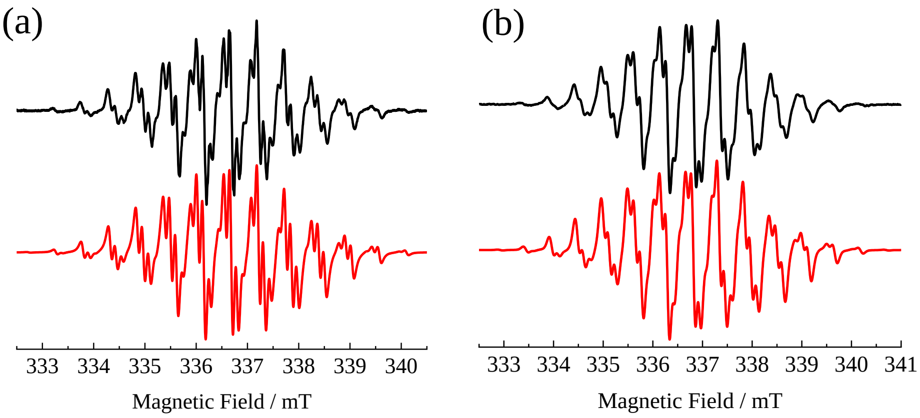

Figure S13. Observed and simulated X-band room temperature ESR spectra of **1*m*** and **1*p*** in the degassed toluene solutions: (a) **1*m*** and (b) **1*p***. The g value and hyperfine coupling constants (A) of the nitrogen nuclei and protons of the methyl groups determined by the spectral simulation are g = 2.0040, $A_{1N}(2)$ = 0.65 mT, $A_{2N}(2)$ = 0.54 mT, and $A_H(6)$ = 0.53 mT for **1*m*** and g = 2.0035, $A_{1N}(2)$ = 0.65 mT, $A_{2N}(2)$ = 0.53 mT, and $A_H(6)$ = 0.515 mT for **1*p***, where the numbers in parentheses denote the number of equivalent nuclei.

Cyclic Voltammetry (CV) Measurements for 1*p*, 1*m*, 4, and TIPS-Pn

Tetra-*n*-butylammonium hexafluorophosphate (TBAPF$_6$, ~0.1 M), purified twice by repeating recrystallizations from ethanol, was used as the supporting electrolyte. Anhydrous dichloromethane (CH$_2$Cl$_2$) was used as the solvent without further purification. CV measurements were carried out by using a multipurpose electrochemical apparatus (Hokuto Dennko HSV-100) under an Ar atmosphere.

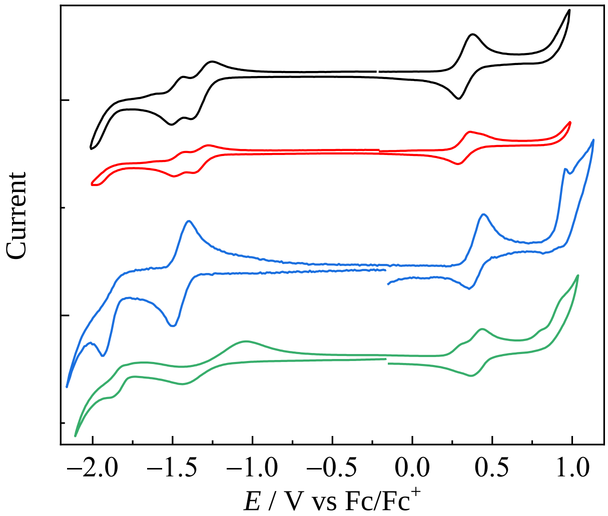

Figure S14. Cyclic voltammogram of **1*m*** (black), **1*p*** (red), TIPS-Pn (blue), and **4** (green) in CH$_2$Cl$_2$ using 0.10 M TBAPF$_6$ as the supporting electrolyte. The concentrations of **1*m***, **1*p***, TIPS-Pn, and **4** were 4.9×10^{-5}, 2.4×10^{-5}, 1.0×10^{-4}, and 1.0×10^{-4} M, respectively. The potentials were measured with respect to the Ag/Ag$^+$ electrode and corrected relative to the potential of Fc/Fc$^+$, the internal standard. Ferrocene (Fc) was added immediately after each measurement. The CV data for **2** and **3** were already reported in our previous work.[S1]

Table S1. Electrochemical data for **1*m***, **1*p***, TIPS-Pn, **2, 3** and **4**.

Derivatives	First Redox Potentials vs. Fc/Fc$^+$ E[Ox] / V	 E[Red] / V
1*m*	0.332	–1.32, –1.47
1*p*	0.322	–1.32, –1.46
TIPS-Pn	0.402	–1.45
2	0.294[S1]	-1.38[S1]
3	0.298[S1]	-1.37[S1]
4	0.405	-1.24

Molecular Orbital Calculations

Molecular orbital calculations for the compounds were performed using the Gaussian 09W.[S5] The molecular structures in the ground state were optimized by the density functional theory (DFT) calculation using the UB3LYP (for **1*m*** and **1*p*** (doublet state)) and B3LYP (for TIPS-pentacene (singlet states)) functionals. The 6-31G(d,p) basis sets were chosen for all calculations. Time-dependent DFT (TD-DFT) calculations were performed on the optimized geometries to estimate the transition energies and oscillator strengths of the compounds. The solvation effect of dichloromethane (CH_2Cl_2) was taken into account by using a polarizable continuum model (PCM).

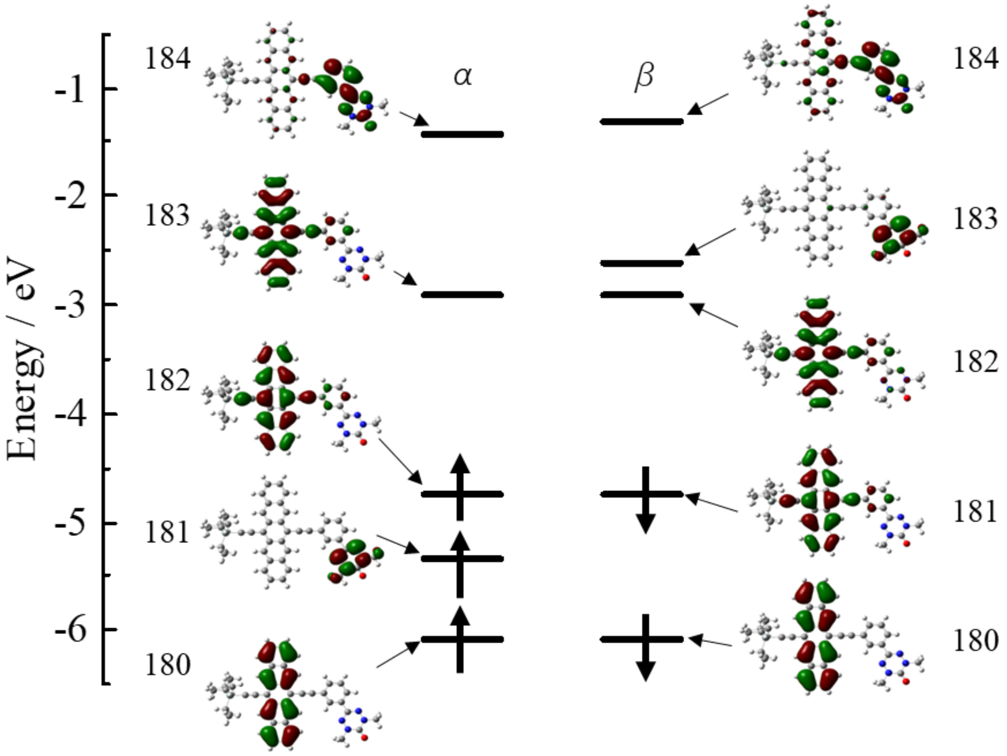

Figure S15. Molecular orbital and energy level diagrams for the doublet electronic ground state of **1*m***.

Table S2. Selected calculated molecular orbital energy of ***1m*** in CH_2Cl_2.

Orbital Number	Molecular Orbital	Energy / eV	Orbital Number	Molecular Orbital	Energy / eV
184 α	α LUMO+1	-1.42914	184 β	β LUMO+1	-1.29771
183 α	α LUMO	-2.90618	183 β	β SOMO	-2.60549
182 α	α HOMO	-4.74240	182 β	β LUMO	-2.91706
181 α	α SOMO	-5.32364	181 β	β HOMO	-4.74648
180 α	α HOMO−1	-6.07658	180 β	β HOMO−1	-6.07603

Total Energy -2324.4168879 hartree

Table S3. Ground to excited state transitions for ***1m*** in CH_2Cl_2.

Excited State	Transition	Energy (Wavelength)	Oscillator Strength
2	182 $\alpha \rightarrow$ 183 α (44%) 181 $\beta \rightarrow$ 182 β (44%) 182 $\alpha \leftarrow$ 183 α (06%) 181 $\beta \leftarrow$ 182 β (06%)	1.5848 eV (782.34 nm)	0.3148
3	181 $\beta \rightarrow$ 183 β	1.8092 eV (685.30 nm)	0.0009
5	179 $\alpha \rightarrow$ 183 α (11%) 181 $\alpha \rightarrow$ 183 α (80%) 179 $\beta \rightarrow$ 182 β (09%)	2.0842 eV (594.88 nm)	0.0035
6	179 $\alpha \rightarrow$ 183 α (17%) 180 $\alpha \rightarrow$ 185 α (06%) 181 $\alpha \rightarrow$ 183 α (08%) 182 $\alpha \rightarrow$ 184 α (07%) 182 $\alpha \rightarrow$ 186 α (09%) 182 $\alpha \rightarrow$ 188 α (03%) 178 $\beta \rightarrow$ 182 β (08%) 179 $\beta \rightarrow$ 182 β (15%) 180 $\beta \rightarrow$ 185 β (06%) 181 $\beta \rightarrow$ 184 β (09%) 181 $\beta \rightarrow$ 186 β (07%) 181 $\beta \rightarrow$ 188 β (03%)	2.2007 eV (563.38 nm)	0.0002
7	181 $\alpha \rightarrow$ 184α (26%) 181 $\alpha \rightarrow$ 186 α (10%)	2.5498 eV (486.25 nm)	0.0028

	182 $\alpha \rightarrow$ 184 α (05%) 178 $\beta \rightarrow$ 182 β (07%) 178 $\beta \rightarrow$ 182 β (23%) 179 $\beta \rightarrow$ 182 β (07%) 179 $\beta \rightarrow$ 183 β (23%)		
8	180 $\alpha \rightarrow$ 183 α (42%) 182 $\alpha \rightarrow$ 185 α (07%) 180 $\beta \rightarrow$ 182 β (42%) 181 $\beta \rightarrow$ 185 β (09%)	2.6305 eV (471.33 nm)	0.0001

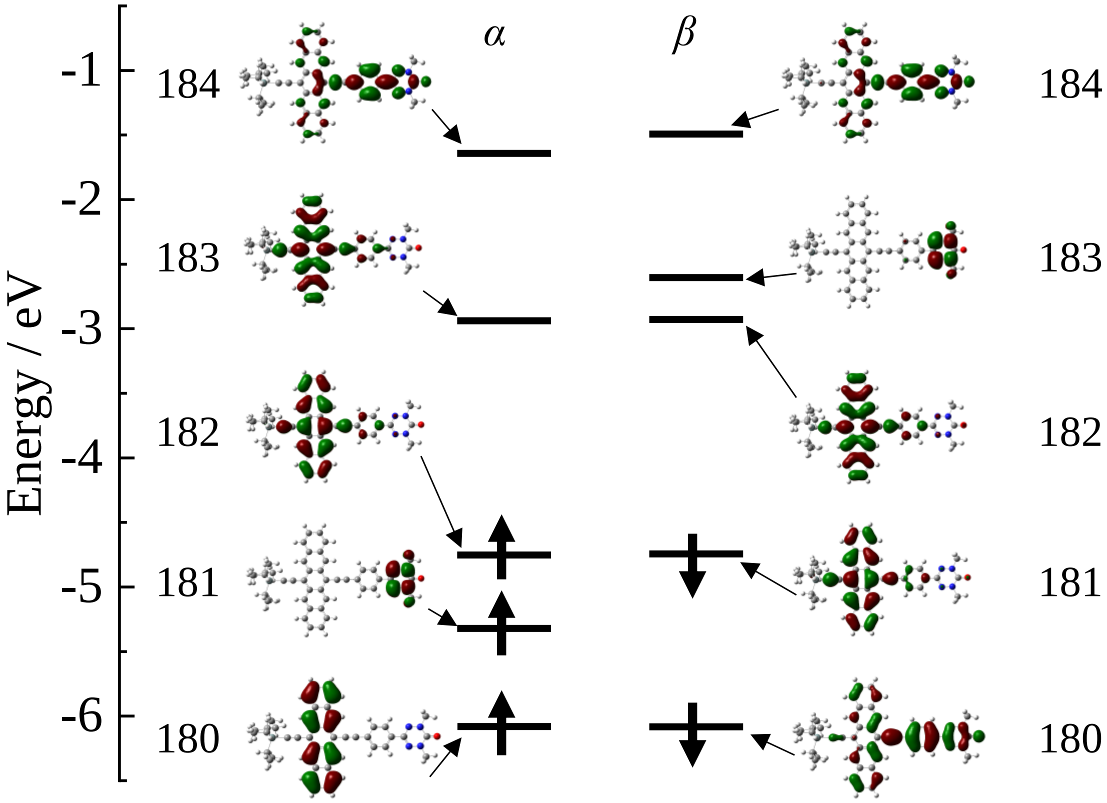

Figure S16. Molecular orbital and energy level diagrams for the doublet electronic ground state of **1*p***.

Table S4. Selected calculated molecular orbital energy for **1*p*** in CH_2Cl_2.

Orbital Number	Molecular Orbital	Energy / eV	Orbital Number	Molecular Orbital	Energy / eV
184 α	α LUMO+1	−1.64139	184 β	β LUMO+1	−1.49336
183 α	α LUMO	−2.93910	183 β	β SOMO	−2.60413
182 α	α HOMO	−4.75029	182 β	β LUMO	−2.92822
181 α	α SOMO	−5.32092	181 β	β HOMO	−4.74431
180 α	α HOMO−1	−6.08012	180 β	β HOMO−1	−6.05862

Total Energy −2324.40441462 hartree

Table S5. Ground to excited state transitions for **1*p*** in CH_2Cl_2.

Excited State	Transition	Energy (Wavelength)	Oscillator Strength
2	182 α → 183 α (44%) 181 β → 182 β (44%) 182 α ← 183 α (6%) 181 β ← 182 β (6%)	1.5669 eV (791.27 nm)	0.3841
3	181 α → 183 α (12%) 181 α → 184 α (8%) 180 β → 183 β (11%) 181 β → 183 β (70%)	1.8238 eV (679.79 nm)	0.0005
4	179 α → 185 α (5%) 180 α → 183 α (24%) 180 α → 184 α (5%) 182 α → 185 α (16%) 179 β → 182 β (24%) 179 β → 184 β (5%) 180 β → 185 β (5%) 181 β → 185 β (17%)	1.8662 eV (664.37 nm)	0.0002
5	181 α → 183 α (65%) 181 α → 184 α (14%) 180 β → 183 β (8%) 181 β → 183 β (14%)	2.0440 eV (606.59 nm)	0.0001
7	181 α → 183 α (12%) 181 α → 184 α (24%) 181 α → 187 α (6%) 174 β → 183 β (7%)	2.5841eV (479.80 nm)	0.0046

	177 $\beta \rightarrow$ 183 β (11%) 180 $\beta \rightarrow$ 183 β (32%) 181 $\beta \rightarrow$ 183 β (7%)		
8	177 $\alpha \rightarrow$ 183 α (6%) 179 $\alpha \rightarrow$ 183 α (20%) 182 $\alpha \rightarrow$ 184 α (36%) 177 $\beta \rightarrow$ 182 β (8%) 180 $\beta \rightarrow$ 182 β (16%) 181 $\beta \rightarrow$ 184 β (13%)	2.6092 eV (475.18 nm)	0.0366

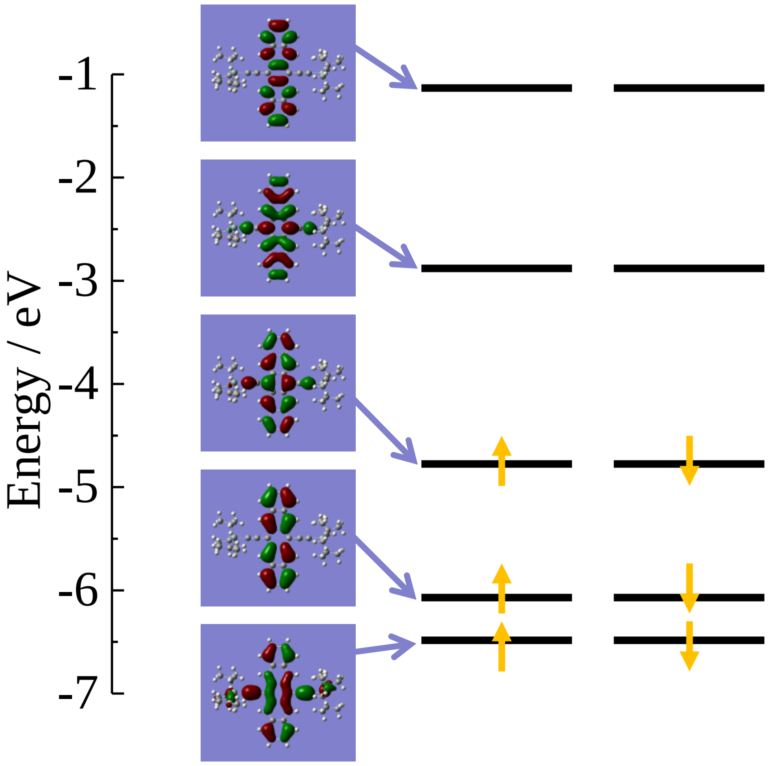

Figure S17. Molecular orbital and energy level diagrams for the singlet electronic ground state of TIPS-Pn.

Table S6. Selected calculated molecular orbital energy of TIPS-Pn in CH_2Cl_2.

Orbital Number	Molecular Orbital	Energy / eV
175	LUMO+1	−1.13308
174	LUMO	−2.88033
173	HOMO	−4.77587
172	HOMO−1	−6.07086
171	HOMO−2	−6.48448

Total Energy −2288.27875224 hartree

Table S7. Ground to excited state transitions for TIPS-Pn in CH_2Cl_2.

Excited State	Transition	Energy (Wavelength)	Oscillator Strength
2	171 →174 (74%) 173 →176 (26%)	1.6402 eV (755.93 nm)	0.2184
8	170 →174 (59%) 173 →177 (41%)	3.0645 eV (404.58 nm)	0.1068
10	171 →174 (74%) 173 →176 (26%)	3.1368 eV (395.26 nm)	0.0805
16	164 →174 (17%) 168 →174 (16%) 169 →174 (67%)	3.4248 eV (362.02 nm)	0.0008
18	163 →174 (16%) 168 →174 (68%) 169 →174 (15%)	3.4655 eV (357.76 nm)	0.0001
19	171 →174 (26%) 173 →176 (74%)	3.5300 eV (351.23 nm)	0.2954

Steady-State Absorption Spectra Measurements and Photochemical Stability Evaluation

The steady-state absorption spectra as well as the time variations of the derivatives were measured in CH_2Cl_2 using a SHIMADZU UV-3600 spectrophotometer. A Xe lamp (USHIO UI-501C, 500 W) was used as the excitation light source to induce the reaction. A light (power: ~70 mW) passed through a H_2O filter and a band-pass filter (λ_{ex} = 650 ± 25 nm for **1*m***, **1*p***, **1*m***pre, **1*p***pre, and TIPS-Pn, or λ_{ex} = 600 ± 25 nm for **2**, **3**, and **4**) was irradiated to the sample solution in CH_2Cl_2 (3.00 mL) using a light guide (LUMATEC Ltd. Series 380). Figure S18 shows the light-irradiation setup. Note that the light irradiation was performed outside of the spectrophotometer, and the solution was stirred using a magnetic stirrer during the irradiation.

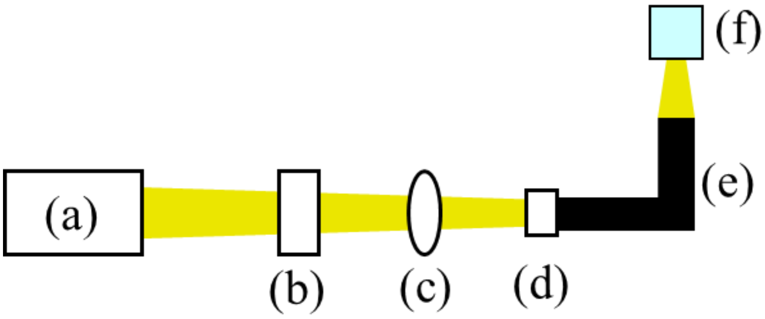

Figure S18. Experimental setup for the photoirradiation: (a) Xe lamp, (b) H_2O filter, (c) biconvex lens, (d) band-pass filter (λ_{ex} = 650 ± 25 nm or λ_{ex} = 600 ± 25 nm), (e) light guide, and (f) sample in CH_2Cl_2.

(i) Steady-State Absorption Spectra and Comparison with the Results of TD-DFT Calculations

In the comparison between the observed and the calculated transitions, the calculation results were horizontally shifted to a higher-energy region by a factor of 1.1 in energy to take into account the underestimation of transition energy by the TD-DFT method.[S6]

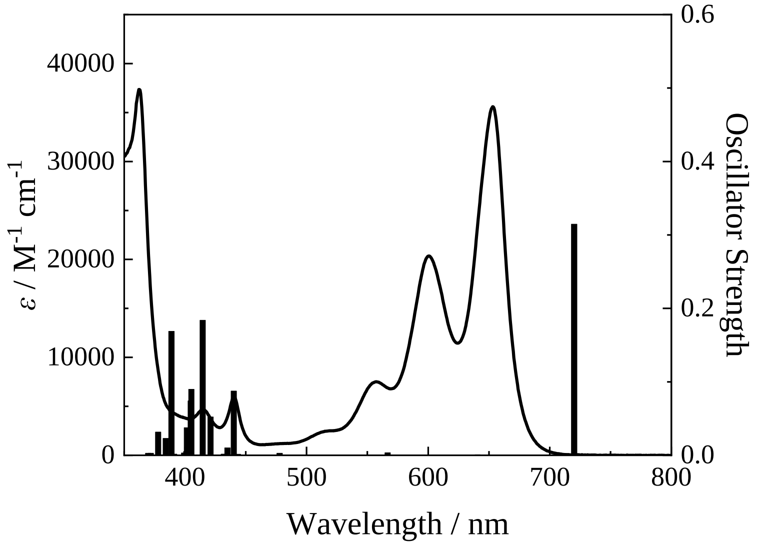

Figure S19. Steady-state absorption spectrum of **1*m*** in CH_2Cl_2 solution at room temperature and the stick spectrum calculated by the TD-DFT method. Vertical bars represent the oscillator strengths for the transitions calculated by the TD-DFT method.

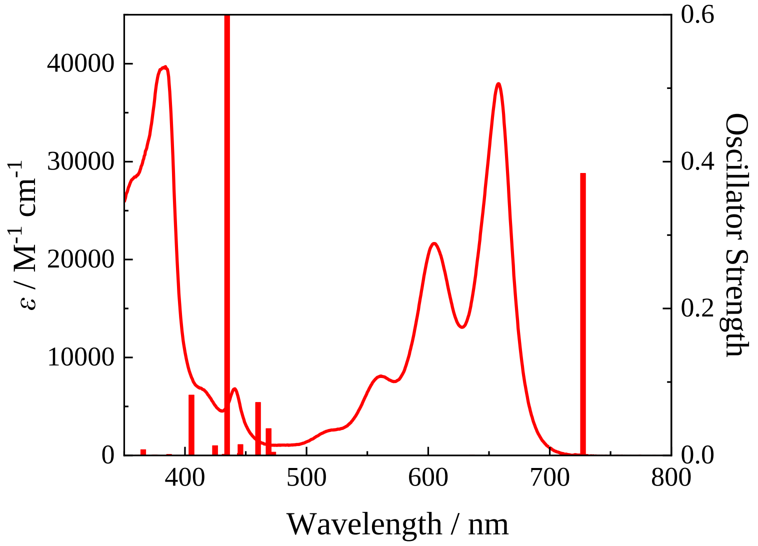

Figure S20. Steady-state absorption spectrum of **1*p*** in CH_2Cl_2 solution at room temperature and the stick spectrum calculated by the TD-DFT method. Vertical bars represent the oscillator strengths for the transitions calculated by the TD-DFT method.

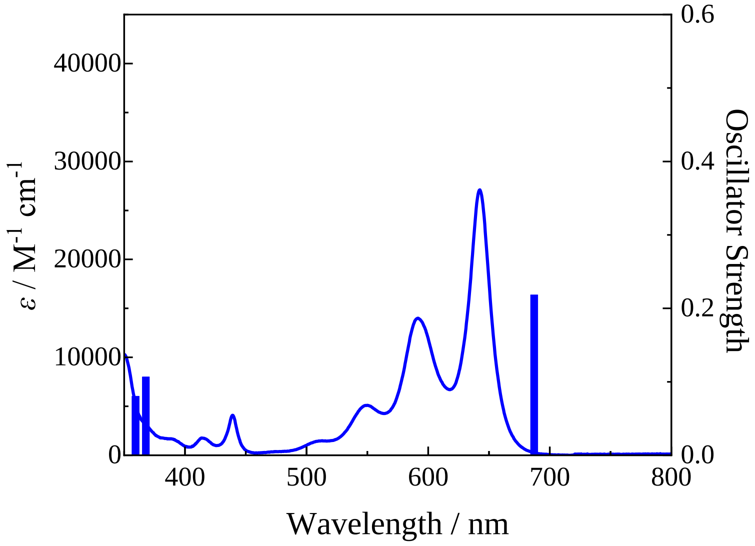

Figure S21. Steady-state absorption spectrum of TIPS-Pn in CH_2Cl_2 solution at room temperature and the stick spectrum calculated by TD-DFT method. Vertical bars represent the oscillator strengths for the transitions calculated by the TD-DFT method.

(ii) Time variation in the absorption spectra of **2**, **3**, **4**, **1*m*pre**, and **1*p*pre**

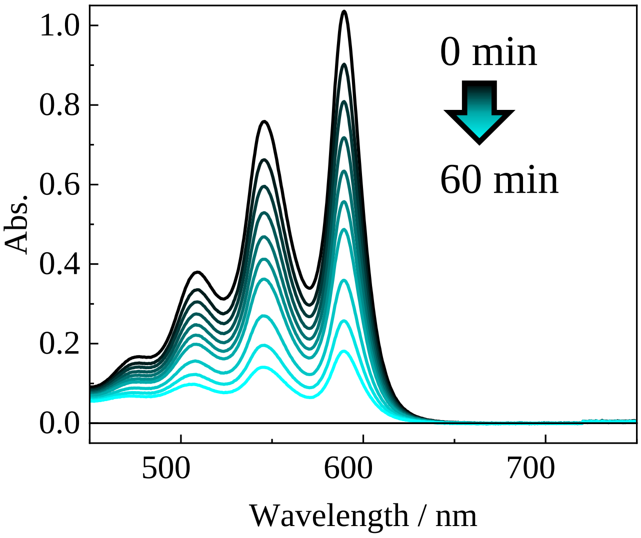

Figure S22. Variations in the absorption spectrum of **2** with time in air-saturated CH_2Cl_2 solution at room temperature. Before light irradiation, the absorbance (*Abs*(0)) value of the solution of **2** was 1.036. The reaction was induced by a light irradiation of power: ~70 mW and wavelength (λ_{ex}) = 600 ± 25 nm).

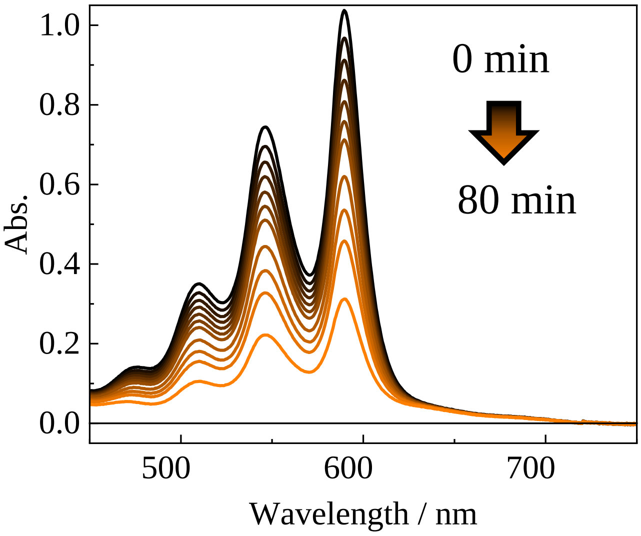

Figure S23. Variation in the absorption spectrum of **3** with time in air-saturated CH_2Cl_2 solution at room temperature. Before light irradiation, the absorbance (*Abs*(0)) value of the solution of **3** was 1.037. The reaction was induced by a light irradiation of power ~70 mW and wavelength (λ_{ex}) = 600 ± 25 nm.

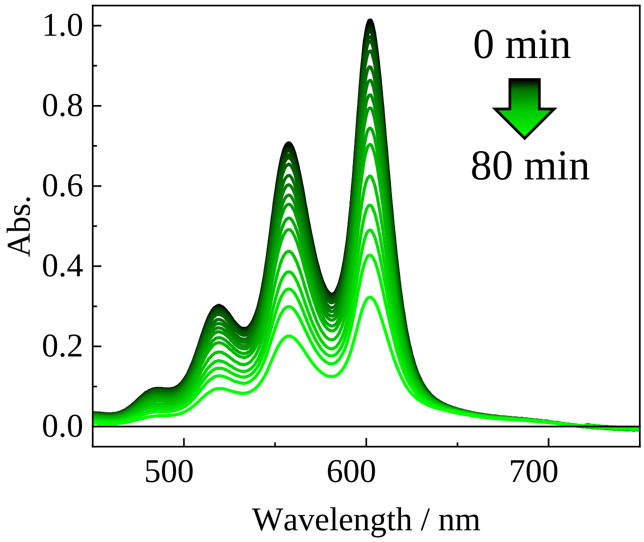

Figure S24. Variation in the absorption spectrum of **4** with time in air-saturated CH_2Cl_2 solution at room temperature. Before light irradiation, the absorbance (*Abs*(0)) value of the solution of **4** was 1.014. The reaction was induced by a light irradiation of power ~70 mW and wavelength (λ_{ex}) = 600 ± 25 nm.

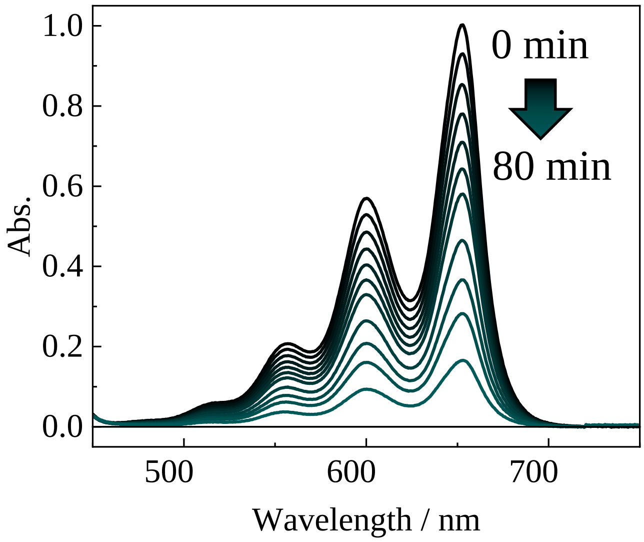

Figure S25. Variation in the absorption spectrum of **1*m***pre (precursor of **1*m***) with time in air-saturated CH_2Cl_2 solution at room temperature. Before light irradiation, the absorbance (*Abs*(0)) value of the solution of **1*m***pre was 1.002. The reaction was induced by a light irradiation of power ~70 mW and wavelength (λ_{ex}) = 650 ± 25 nm.

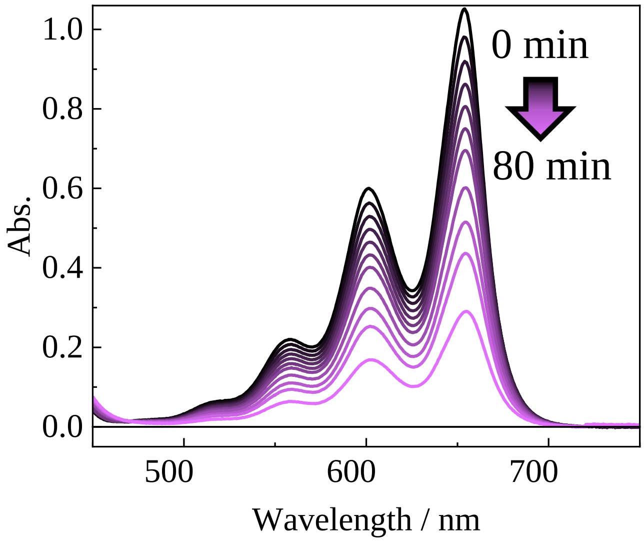

Figure S26. Variation in the absorption spectrum of **1*p***pre (precursor of **1*p***) with time in air-saturated CH_2Cl_2 solution at room temperature. Before light irradiation, the absorbance (*Abs*(0)) value of the solution of **1*p***pre was 1.052. The reaction was induced by a light irradiation of power ~70 mW and wavelength (λ_{ex}) = 650 ± 25 nm.

(iii) Photochemical stabilities of **1*m***, **1*p***, and their precursors (**1*m***pre and **1*p***pre)

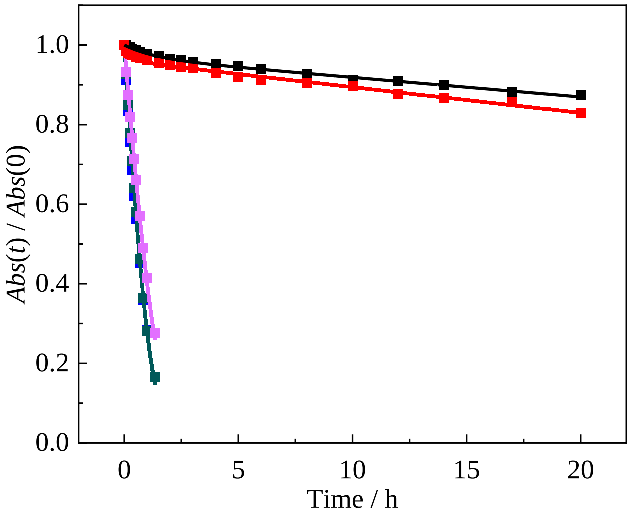

Figure S27. Comparison of photochemical stability between **1*m***, **1*p***, and their precursors (**1*m***pre and **1*p***pre) by the irradiation of a light of λ_{ex} = 650 ± 25 nm (power: ~70 mW). Time variations in absorbance of the peaks in 1←0 transition for **1*m*** (black), **1*p*** (red), **1*m***pre (green), and **1*p***pre (purple). Their curve fittings were obtained by using eqn (1) for **1*m***pre, and **1*p***pre and eqn (2) for **1*m***, and **1*p***. *Abs*(0) values of **1*m***, **1*p***, **1*m***pre, and **1*p***pre were 1.001, 1.013, 1.002, and 1.052, respectively.

Transient Absorption Measurement and Spectra of 1*m*, 1*p*, 1*m*pre, 1*p*pre, and TIPS-Pn

Femtosecond transient absorption experiments were performed using a mode-locked Ti:Sapphire laser (Spectra-Physics Hurricane-X, 800 nm, FWHM ~ 100 fs, repetition rate = 1 kHz, 1 mJ/pulse) where the output pulses were divided into the pump and probe light. The pump pulses were converted to 658-nm or 653-nm light using an optical parametric amplifier (Spectra-Physics OPA-800C). A white continuum light (430-750 nm) was produced in the sapphire plate using a portion of the amplified 800 nm beam and used as probe. The probe light was detected with an NMOS linear imaging sensor (Hamamatsu S3903-1024Q, 1024 pixels) through an imaging spectrometer (Princeton Instruments, Acton SP275i). Chirp correction was also performed using sapphire or glass plates on the sample position by the pump-probe experiment (653 nm pump light). The details of the experimental setup for the pump–probe measurements are described in the literature.[S7, S8] Transient absorption spectra at longer delay times (> ns) were measured using a nanosecond pump-probe spectrometer (Ultrafast Systems, EOS-Vis/NIR). The white continuum probe pulse (400~1600 nm) was generated in a photonic crystal fiber pumped by the femtosecond laser. The pump-probe delay time (50 ps ~ 50 μs) was electronically controlled with a 1 ns temporal resolution. For the transient absorption measurements of **1*m***, **1*p***, **1*m***pre, **1*p***pre, and TIPS-Pn, dichloromethane was used as a solvent, which was purified by column chromatography (Merck basic aluminum, particle size: 0.063-0.200 mm, pH = 8.5-10.5). The concentration of the sample was adjusted to the absorbance of the π–π* transition near 650 nm to ~ 0.3, and the dissolved oxygen in the solutions was removed by Ar bubbling. All the spectroscopic measurements were conducted at room temperature using covered optical cells with a 2-mm optical path length. The obtained lifetimes of **1*m***, **1*p***, and TIPS-Pn are listed in Table 2 in the main text. The lifetimes of **1*m***pre and **1*p***pre determined by the global fit at the TrA peaks (448 nm and 501 nm for **1*m***pre and 450 nm and 500 nm for **1*p***pre) are given in Table S8.

Table S8. Lifetimes (τ_S and τ_T) of the singlet and triplet states of the Pn moiety of **1*m***pre and **1*p***pre **1*p*** in CH_2Cl_2.

	1*m*pre	**1*p***pre
τ_S	7.35 ns (0.04 ns[a])	6.81 ns (0.03 ns[a])
τ_T	6.74 μs (0.01 μs[a])	6.52 μs (0.60 μs[a])

[a] Standard error of fit.

(i) Transient absorption spectra of **1*m*** and **1*p***

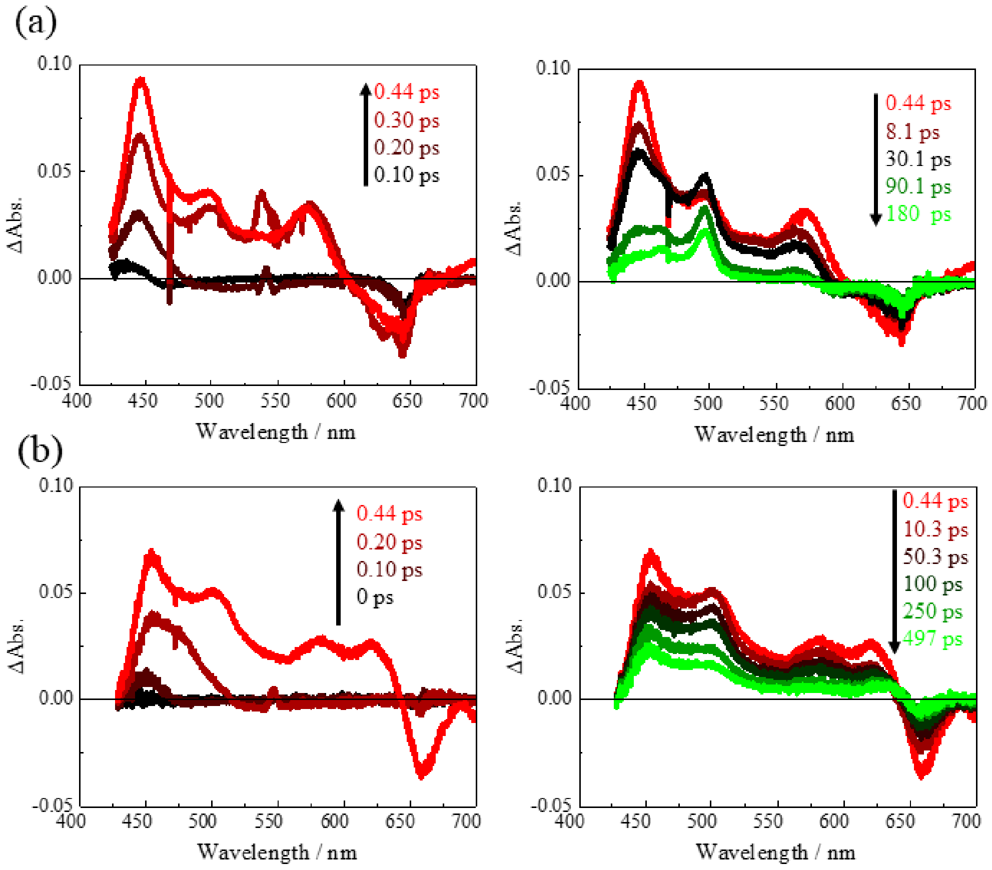

Figure S28. Time course of transient absorption spectra of **1*m*** (a) and **1*p*** (b).

(ii) Transient absorption spectra of **1*m***pre, **1*p***pre, and TIPS-Pn

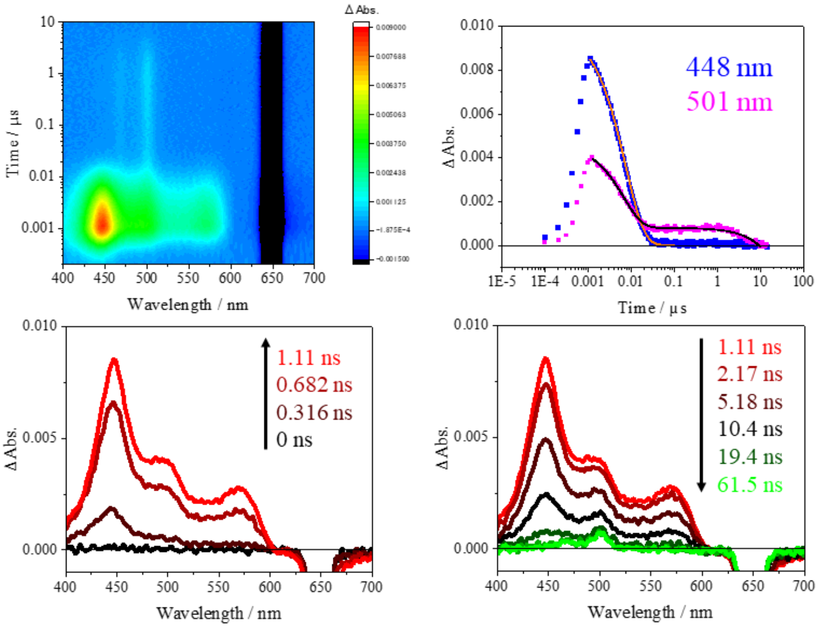

Figure S29. Time course of transient absorption spectra of **1*m***pre.

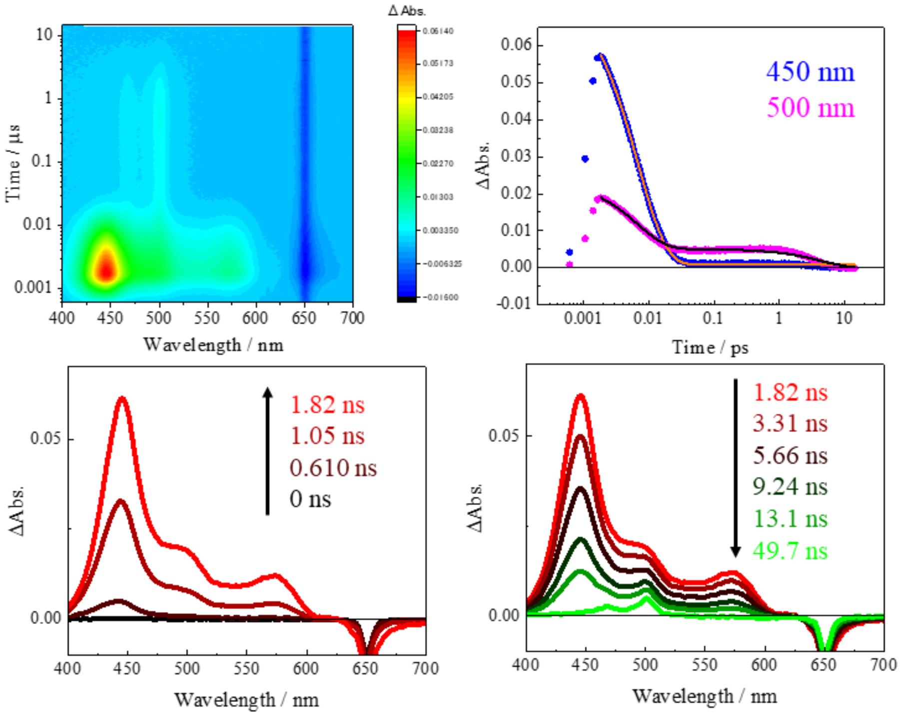

Figure S30. Time course of transient absorption spectra of **1*p***pre.

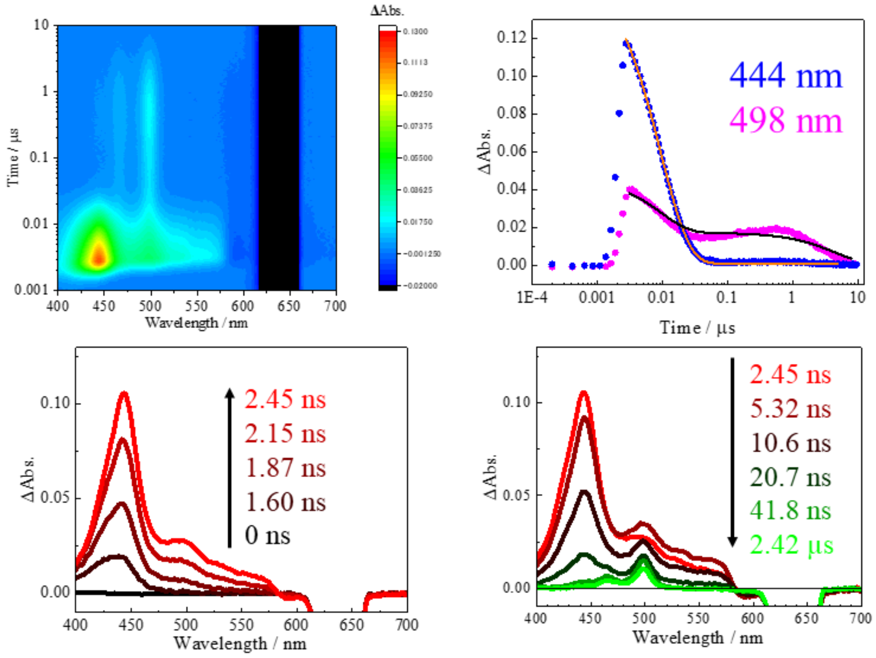

Figure S31. Time course of transient absorption spectra of **TIPS-Pn**

Time Course of the Transitions for 1*m* at 497 nm and 1*p* at 501 nm

The time course of the transition of **1*m*** at 497 nm was reproduced using three exponential functions ($\Delta A = C_1\exp(-t/\tau_S) + C_2\exp(-t/\tau_2) + C_3\exp(-t/\tau_3)$), in which one coefficient (C_2) was negative sign and the lifetime of the first term (τ_S) was fixed at 537 fs (see Table 2 in the main text) which is the decay time of the singlet excited state of the pentacene moiety (^{1}Pn*). In the wavelength region with a relatively large molar absorption coefficient of ^{3}Pn*, a negative sign is possible. However, the characteristic time constant (τ_2) was ca. 31 ± 2 ps, which is much longer than the singlet decay time (τ_S), indicating the existence of an indirect pathway from ^{1}Pn* to ^{3}Pn*. In addition, the decay time (τ_3) at this wavelength was ~ 128 ps, which is longer than the triplet lifetime ($\langle\tau_T\rangle = 49 \pm 1$ ps) determined from the breach recovery at 644 nm (see Table 2 in the main text). Similar behavior was observed in the transition of **1*p*** at 501 nm. In this case, τ_S was fixed to be 135 fs (see Table 2 in the main text) and τ_2 was ca. 3 ps, which is also much longer than the singlet decay time (τ_S). τ_3 of **1*p*** at this wavelength was ~ 163 ± 2 ps, which is also longer than the triplet lifetime ($\langle\tau_T\rangle = 74 \pm 2$ ps) determined from the breach recovery. One plausible explanation is the existence of an indirect pathway to ^{3}Pn* as shown in Figure S33.

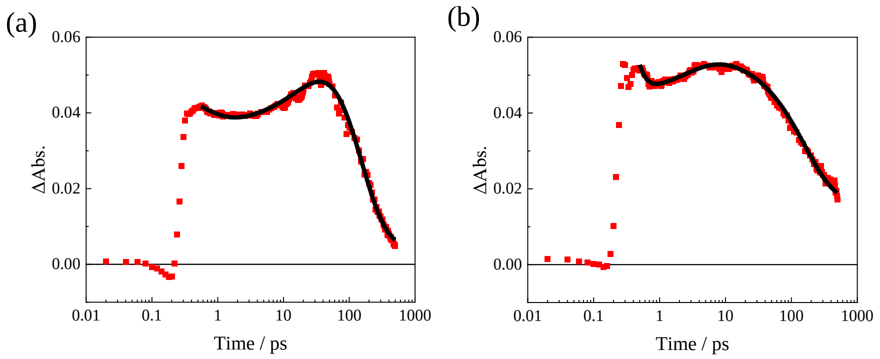

Figure S32. Time courses of transient absorption spectra. (a) **1*m*** at 497 nm and (b) **1*p*** at 501 nm corresponding to the peak of the transient absorption of ^{3}Pn*.

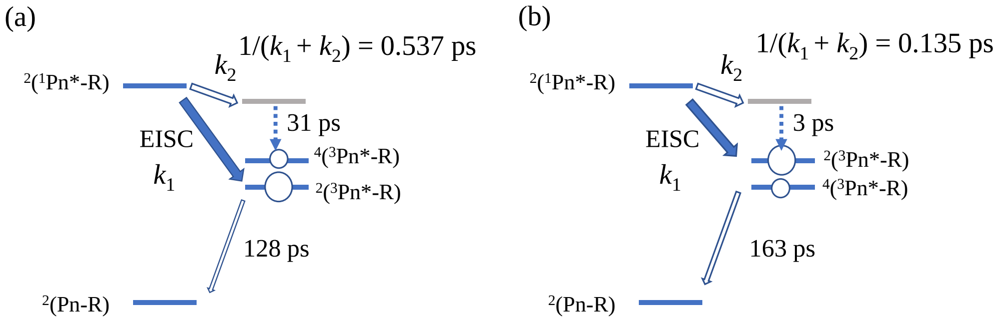

Figure S33. Plausible explanation for (a) **1*m*** at 497 nm and (b) **1*p*** at 501 nm.

Analytical Solutions for the rate equations of Expected Kinetics

According to the time course of the transient absorption of **1*m*** at 497 nm and **1*p*** at 501 nm, the indirect pathway from ${}^2({}^1\mathrm{Pn}^*\text{-R})$ to ${}^{2,4}({}^3\mathrm{Pn}^*\text{-R})$ is expected in both cases as shown in Figure S33. For simplicity, when we focus on the Pn moiety, the following processes are expected for the excited state:

$$ {}^1\mathrm{Pn}^*\ (\mathrm{S}_1) \xrightarrow{k_1} {}^3\mathrm{Pn}\ (\mathrm{T}_1) \xrightarrow{k_\mathrm{T}} {}^3\mathrm{Pn}\ (\mathrm{T}_1) \qquad \text{(S1a)} $$

$$ {}^1\mathrm{Pn}^*\ (\mathrm{S}_1) \xrightarrow{k_1} {}^3\mathrm{Pn}\ (\mathrm{T}_2) \xrightarrow{k_\mathrm{TT}} {}^3\mathrm{Pn}\ (\mathrm{T}_1) \xrightarrow{k_\mathrm{T}} {}^3\mathrm{Pn}\ (\mathrm{T}_1) \qquad \text{(S1b)} $$

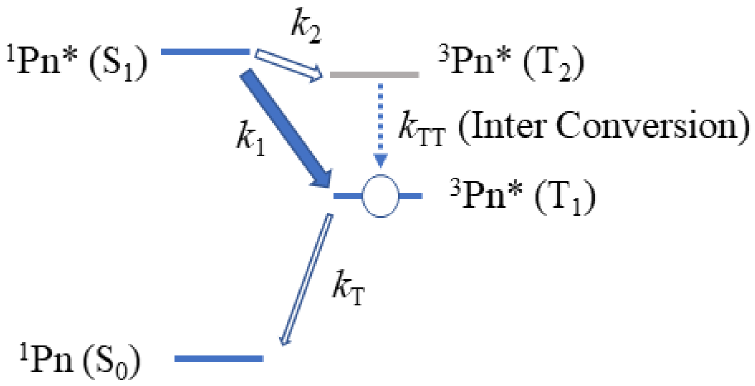

Figure S34. Expected excited state dynamics of Pn moiety.

The rate equations corresponding to (S1) are given by

$$ d[{}^1Pn^*]_t/dt = -(k_1+k_2)[{}^1Pn^*]_t = -k_\mathrm{S}[{}^1Pn^*]_t \qquad \text{(S2a)} $$

$$ d[{}^3Pn^*(T_2)]_t/dt = k_\mathrm{S}[{}^1Pn^*]_t - k_\mathrm{TT}[{}^3Pn^*(T_2)]_t \qquad \text{(S2b)} $$

$$ d[{}^3Pn^*(T_1)]_t/dt = k_1[{}^1Pn^*]_t + k_\mathrm{TT}[{}^3Pn^*(T_2)]_t - k_\mathrm{T}[{}^3Pn^*(T_1)]_t \qquad \text{(S2c)} $$

The population density of each spin state under the boundary conditions ($[{}^1Pn^*]_0 = I_0$, $[{}^3Pn^*(T_2)]_0 = [{}^3Pn^*(T_1)]_0 = 0$) can be obtained by solving eqn (S2).

$$ [{}^1Pn^*]_t = I_0 exp(-k_\mathrm{S}t) \qquad \text{(S3a)} $$

$$ [{}^3Pn^*(T_2)]_t = -aI_0\{exp(-k_\mathrm{S}t) - exp(-k_\mathrm{TT}t)\} \qquad \text{(S3b)} $$

$$ [{}^3Pn^*(T_1)]_t = -I_0[c(1 - k_\mathrm{TT}a/k_1)exp(-k_\mathrm{S}t) + abexp(-k_\mathrm{TT}t) - \{c(1 - k_\mathrm{TT}a/k_1) + ab\}exp(-k_\mathrm{T}t)], \qquad \text{(S3c)} $$

where $a = k_2/(k_\mathrm{S} - k_\mathrm{TT})$, $b = k_\mathrm{TT}/(k_\mathrm{TT} - k_\mathrm{S})$, and $c = k_1/(k_\mathrm{S} - k_\mathrm{T})$.

The contributions of both ^{1}Pn*, ^{3}Pn*(T$_2$) and ^{3}Pn*(T$_1$) to the transient absorption signal are included. The time course of the transient absorption at the wavelength λ is derived using Eq. (S4) from Eqs. (S3a-b).

$$\begin{aligned}\Delta\mathrm{Abs}(\lambda)_t &= \varepsilon_{S_1}(\lambda)\left[\,^1Pn^*\right]_t l + \varepsilon_{T_2}(\lambda)\left[\,^3Pn^*(T_2)\right]_t l + \varepsilon_{T_1}(\lambda)\left[\,^3Pn^*(T_1)\right]_t l \\ &= A_S(\lambda)exp(-k_S t) + A_{TT}(\lambda)exp(-k_{\mathrm{TT}}t) + A_T(\lambda)exp(-k_{\mathrm{T}}t) \qquad \text{(S4)}\end{aligned}$$

where $\varepsilon_{S_1}(\lambda)$, $\varepsilon_{T_2}(\lambda)$, and $\varepsilon_{T_1}(\lambda)$ are the molar absorption coefficients of the ^{1}Pn* (S$_1$), ^{3}Pn* (T$_2$), and ^{3}Pn* (T$_1$), respectively. *l* is the cell length and $A_S(\lambda)$, $A_{TT}(\lambda)$, and $A_T(\lambda)$, which correspond to the amplitude of each exponential decay with the rate constants (k_1, k_{TT}, and k_{T}), are given as follows:

$$A_S(\lambda) = \left\{\varepsilon_{S_1}(\lambda) - a\varepsilon_{T_2}(\lambda) - c(1 - k_{\mathrm{TT}}a/k_1)\varepsilon_{T_1}(\lambda)\right\}I_0 l \qquad \text{(S5a)}$$

$$A_{TT}(\lambda) = \left\{a\left(\varepsilon_{T_2}(\lambda) - b\varepsilon_{T_1}(\lambda)\right)\right\}I_0 l \qquad \text{(S5b)}$$

$$A_T(\lambda) = \{c(1 - k_{\mathrm{TT}}a/k_1) + ab\}\varepsilon_{T_1}(\lambda)I_0 l \qquad \text{(S5c)}$$

For the breach signal,

$$\begin{aligned}\Delta\mathrm{Abs}(\lambda)_t^{Br} &= -\varepsilon_G(\lambda)\left(\left[\,^1Pn^*\right]_t + \left[\,^3Pn^*(T_2)\right]_t + \left[\,^3Pn^*(T_1)\right]_t\right) l \\ &= A_S^{Br}(\lambda)exp(-k_S t) + A_{TT}^{Br}(\lambda)exp(-k_{\mathrm{TT}}t) + A_T^{Br}(\lambda)exp(-k_{\mathrm{T}}t) \qquad \text{(S6)}\end{aligned}$$

where $\varepsilon_G(\lambda)$ is the molar absorption coefficients of the ground state of Pn, and

$$A_S^{Br}(\lambda) = -\varepsilon_G(\lambda)\{1 - a - c(1 - k_{\mathrm{TT}}a/k_1)\}I_0 l \qquad \text{(S7a)}$$

$$A_{TT}^{Br}(\lambda) = -\varepsilon_G(\lambda)a(1 - b)I_0 l \qquad \text{(S7b)}$$

$$A_T^{Br}(\lambda) = -\varepsilon_G(\lambda)(c - k_{\mathrm{TT}}ac/k_1 + ab)I_0 l \qquad \text{(S7c)}$$

When k_1 >> k_{TT} >> k_{T}. the triplet decay lifetime (τ_{T} = 1/ k_{T}) can be estimated from a single exponential fit using the data omitted early time region. The lifetime estimation using a single exponential fit provides the average recovery time of the breach even when the condition (k_1 >> k_{TT} >> k_{T}) is not sufficiently satisfied.

Expected mechanism for the ultrafast quenching of the photoexcited states

In this section, we discuss first the EISC mechanism based on the theory reported by Ake and Gouterman [S9] and then, we propose the possible mechanism for the ultrafast quenching of the photoexcited states of **1*m*** and **1*p***. It should be noted that the Ake-Gouterman's theory is based on the first-order perturbation treatment. The correspondence of their notation to our pentacene-radical linked systems is as follows.

Ground state ($^2\psi_0$) : ^{2}(^{1}Pn-R) , sing-doublet ($^2\psi_1$) : ^{2}(^{1}Pn*-R) ,
trip-doublet ($^2\psi_2$) : ^{2}(^{3}Pn*-R) , quartet ($^4\psi_1$) : ^{4}(^{3}Pn*-R) ,
orbital a : half-filled 'HOMO' orbital on the excited chromophore (Pn*) ,
orbital b : half-filled 'LUMO' orbital on the excited chromophore (Pn*),
orbital m : SOMO of the radical substituent (R)

Because of electronic interaction, there is a coupling term between the sing-doublet and the trip-doublet

$$< {}^2\psi_1 | \, e^2/r_{12} | \, {}^2\psi_2 > \; = \; \sqrt{3/4}\,(K_{bm} - K_{am}). \qquad \text{(S8)}$$

where $K_{bm}(K_{am})$ is the electron exchange integral between the two electrons in half-filled orbitals on the excited chromophore and and the unpaired electron on the radical SOMO. This term leads to the EISC between the sing-doublet and the trip-doublet. When the energy separation (ΔE_{12}) between the two doublet states is large compared to the coupling term, the first-order perturbation theory is applicable giving the new wave functions

$$| \, {}^2\psi_2{}' > \; = \; | \, {}^2\psi_2 > + \frac{\sqrt{3}}{2}\frac{(K_{bm}-K_{am})}{\Delta E_{12}} | \, {}^2\psi_1 >, \qquad \text{(S9)}$$

where $\Delta E_{12} = E({}^2\psi_1) - E({}^2\psi_2)$. The transition dipole between the quartet and the ground state is

$$< {}^2\psi_0 | e\boldsymbol{r} | \, {}^2\psi_2{}' > \; = \; \frac{\sqrt{3}}{2}\frac{(K_{bm}-K_{am})}{\Delta E_{12}} < {}^2\psi_0 | e\boldsymbol{r} | \, {}^2\psi_1 > = \frac{\sqrt{3}}{2}\frac{(K_{bm}-K_{am})}{\Delta E_{12}} \boldsymbol{q}_{ab}, \qquad \text{(S10)}$$

where $\boldsymbol{q}_{ab}$ is the transition dipole from the ground state to the sing-doublet state. Therefore, the intensity of the absorption from the ground state to the trip-doublet state is enhanced as follows.

$$I_{02} \sim \frac{3}{4}\left|\frac{K_{bm}-K_{am}}{\Delta E_{12}}\right|^2 \boldsymbol{q}_{ab}^2 \sim \frac{3}{4}\left|\frac{K_{bm}-K_{am}}{\Delta E_{12}}\right|^2 \frac{E_2}{E_1} I_{01} \qquad \text{(S11)}$$

where I_{01} is the transition intensity from the ground state to the sing-doublet state. This term increases the oscillator strength of the ground state to trip-doublet absorption.

Based on the above theory, we discuss first for the EISC in our systems. Equation (S8) shows that the difference in the exchange interactions between the unpaired electron on the radical and the two electrons in half-filled orbitals on the excited chromophore leads to the EISC between sing-doublet and trip-doublet states. To clarify the difference in the exchange interactions, we carried out the DFT calculation of the photoexcited quartet state of **1*p***, because the quartet state has the information about the SOMO on the radical and the half-filled orbitals on the excited chromophore. Figure S35 show their one-electron molecular orbitals and the spin density distributions of the quartet state.

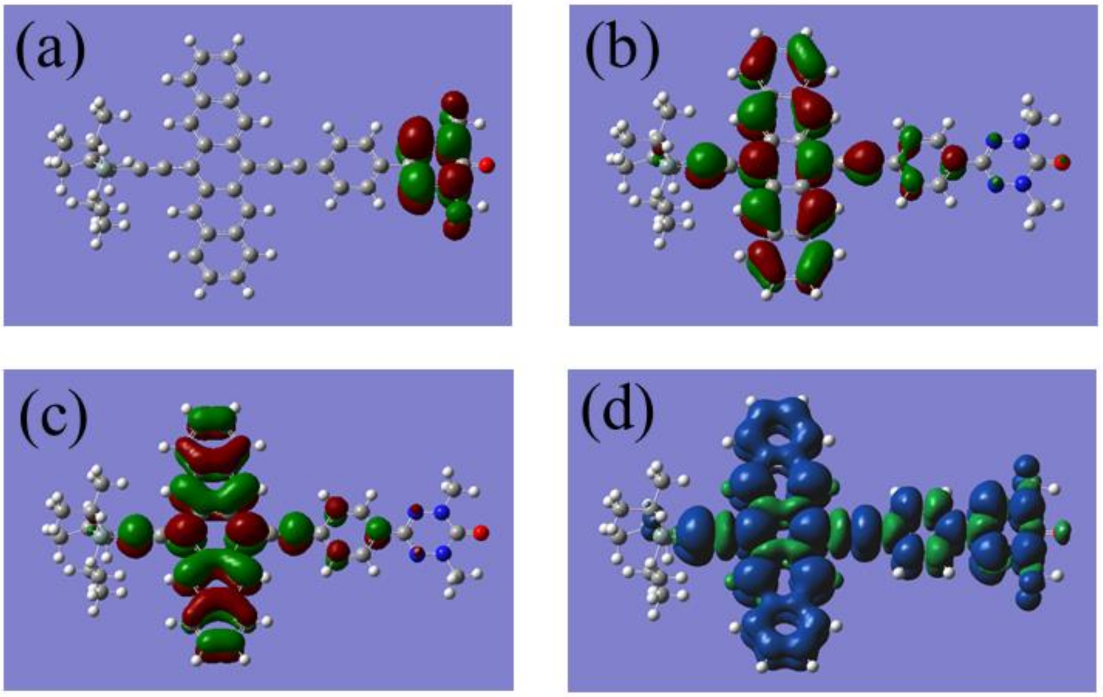

Figure S35. One-electron molecular orbitals of (a) SOMO of the radical, (b) half-filed 'HOMO' of Pn*, (c) half-filed 'LUMO' of Pn*, and the spin density distributions of the quartet state.

The molecular orbitals of the half-filled orbitals on the excited chromophore are delocalized to the radical moiety owing to the effective π-conjugation as the result to the molecular planarity. This finding shows that the large magnitude of the exchange integrals is expected between the unpaired electron on the radical and the two electrons in half-filled orbitals on the excited chromophore (Pn*). Futhermore, the signs of the orbital coeficients of their half-filled orbitals (Figures 35(b) and 35(c)) on the atoms belong to the radical moiety are deferent to each other. This leads to the difference between K_{am} and K_{bm}. Therefore, according to the equation (S8), the very effective EISC is predicted between $^{2}(^{1}\mathrm{Pn}^{*}\text{-R})$ and $^{2}(^{3}\mathrm{Pn}^{*}\text{-R})$ in **1*p***. The similar situations are expected to hold in **1*m***. The experimental findings of **1*m*** and **1*p*** show that the transition from $^{3}\mathrm{Pn}^{*}$ to $^{1}\mathrm{Pn}$ is significantly accelerated by the radical substituent. The averaged lifetime ($<\tau_{\mathrm{T}}>$) of **1*m*** (**1*p***) was ca. 8.8×10^{4} (5.8×10^{4}) times shorter than τ_{T} of TIPS-Pn and was ca. 1.4×10^{5} (8.8×10^{4}) times shorter than τ_{T} of their precursors. It should be noted that $<\tau_{\mathrm{T}}>$ of **1*m*** (**1*p***) was ca. 193 (127) times shorter than τ_{S} of times of TIPS-Pn and was ca. 150 (92) times shorter than τ_{S} of their precursors. According to the

Ake-Gouterman's theory, the enhanced transition dipole between the quartet and the ground state is given by the equation (S10) and the magnitude is smaller than the $\boldsymbol{q}_{ab}$, which is the transition dipole from the ground state to the sing-doublet state, because ΔE_{12} is larger than the coupling term, $< {}^{2}\psi_1 | \, e^2/r_{12} | \, {}^{2}\psi_2 >$. Therefore, $<\tau_T>$ even after the acceleration of the transition by the enhancement of the oscillator strength should be longer than the τ_S of their precursors. Thus, the much shorter $<\tau_T>$ of **1*m*** (**1*p***) cannot be explained by the Ake-Gouterman's perturbation theory. This may be originated from the violation of the perturbation condition. The following simultaneous intramolecular double electron transfer depicted in Figure S36 is a possible mechanism to understand the ultrafast quenching of the photoexcited states of **1*m*** and **1*p***, ^{2,4}(^{3}Pn*-R). In a silicon phthalocyanine (SiPc) covalently linked to a nitroxide radical, a similar simultaneous electron transfer was proposed as the double electron exchange mechanism.[S10]

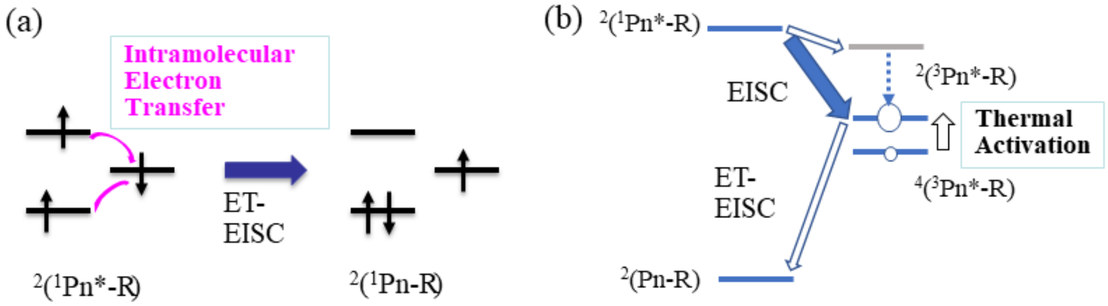

Figure S36. Simultaneous intramolecular double electron transfer mechanism. (a) Ultrafast quenching of ^{2}(^{3}Pn*-R), (b) Ultrafast quenching of ^{4}(^{3}Pn*-R) through the thermal activation.

Figure 36(a) shows the ultrafast quenching mechanism of ^{2}(^{3}Pn*-R) by the simultaneous intramolecular double electron transfer. This process corresponds to the second order process in the perturbation theory. In the perturbation theory, the transition probability owing to the exchange integral terms is roughly given by

$$P_{02} \sim |K_{bm}K_{am}/(\Delta E_{12}\Delta E_{02})|^2 . \qquad \text{(S12)}$$

However, under the violation of the perturbation condition, this second-order term leads to a dominant effect overcoming the first-order term leading to the equation (S11). Furthermore, the spatial overlap between half-filled half-filled orbitals of Pn* and SOMO of R will accelerate the intramolecular electron transfer between them. When the EISC process from ^{2}(^{1}Pn*-R) to ^{2}(^{3}Pn*-R) is much faster than other process, the population of ^{2}(^{1}Pn*-R) is transferred dominantly to ^{2}(^{3}Pn*-R), leading to the negligible population of the quartet state, ^{4}(^{3}Pn*-R). Furthermore, ^{4}(^{3}Pn*-R) is expected to decay quickly through the thermal activation process as shown in Figure S36(b).[S11] The quartet photoexcited state of **1*p*** was not detected in even at the low temperature (30 K) by a time-resolved ESR measurement using BuCN glass matrix. This finding supports the above ultrafast quenching process of ^{2}(^{3}Pn*-R) and ^{4}(^{3}Pn*-R).

References

S1. Y. Kawanaka, A. Shimizu, T. Shinada, R. Tanaka and Y. Teki, *Angew Chem Int Edit*, 2013, **52**, 6643-6647.

S2. A. Shimizu, A. Ito and Y. Teki, *Chem Commun (Camb)*, 2016, **52**, 2889-2892.

S3. D. Lehnherr, R. McDonald and R. R. Tykwinski, *Org Lett*, 2008, **10**, 4163-4166.

S4. E. T. Chernick, R. Casillas, J. Zirzlmeier, D. M. Gardner, M. Gruber, H. Kropp, K. Meyer, M. R. Wasielewski, D. M. Guldi and R. R. Tykwinski, *J Am Chem Soc*, 2015, **137**, 857-863.

S5. J. M. Frisch, W. G. Trucks, B. H. Schlegel, E. G. Scuseria, A. M. Robb, R. J. Cheeseman, G. Scalmani, V. Barone, B. Mennucci, A. G. Petersson, H. Nakatsuji, M. Caricato, P. H. H. X. Li, F. A. Izmaylov, J. Bloino, G. Zheng, L. J. Sonnenberg, M. Hada, M. Ehara, K. Toyota, R. Fukuda, J. Hasegawa, M. Ishida, T. Nakajima, Y. Honda, O. Kitao, H. Nakai, A. J. T. Vreven, J. Montgomery, E. J. Peralta, F. Ogliaro, M. Bearpark, J. J. Heyd, E. Brothers, N. K. Kudin, N. V. Staroverov, R. Kobayashi, J. Normand, K. Raghavachari, A. Rendell, C. J. Burant, S. S. Iyengar, J. Tomasi, M. Cossi, N. Rega, M. J. Millam, M. Klene, E. J. Knox, B. J. Cross, V. Bakken, C. Adamo, J. Jaramillo, R. Gomperts, E. R. Stratmann, O. Yazyev, J. A. Austin, R. Cammi, C. Pomelli, W. J. Ochterski, L. R. Martin, K. Morokuma, G. V. Zakrzewski, A. G. Voth, P. Salvador, J. J. Dannenberg, S. Dapprich, D. A. Daniels, O. Farkas, B. J. Foresman, V. J. Ortiz, J. Cioslowski and J. D. Fox, *Gaussian 09 User's Reference,Gaussian, Inc.*, 2009.

S6. Y. Kurashige, T. Nakajima, S. Kurashige, K. Hirao and Y. Nishikitani, *J Phys Chem A*, 2007, **111**, 5544-5548.

S7. D. Kosumi, T. Kusumoto, R. Fujii, M. Sugisaki, Y. Iinuma, N. Oka, Y. Takaesu, T. Taira, M. Iha, H. A. Frank and H. Hashimoto, *Chemical Physics Letters*, 2009, **483**, 95-100.

S8. D. Kosumi, K. Abe, H. Karasawa, M. Fujiwara, R. J. Cogdell, H. Hashimoto and M. Yoshizawa, *Chemical Physics*, 2010, **373**, 33-37.

S9. R. L. Ake and M. Gouterman, *Theoret. chim. Acta (Berl.)* 1969, **15**, 20.

S10. G. I. Likhtenstein, K. Ishii and S. Nakatsuji, *Photochem Photobiol*, 2007, **83**, 871.

S11. A. Ito, M. Hinoshita, K. Kato and Y. Teki, *Chem Lett*, 2016, **45**, 1324-1326.